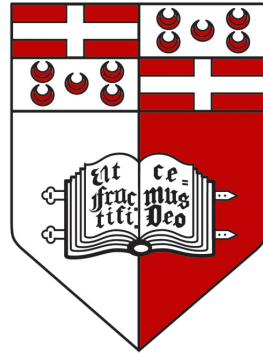


Image Processing Techniques for Brain Haemorrhage Detection in Head CT Scans

John Napier

Supervisor: Prof. Ing. Carl James Debono

Co-supervisors: Dr. Paul Bezzina, Dr. Francis Zarb



Faculty of Information and Communication Technology

Department of Communications and Computer

Engineering

University of Malta

May 2017

*Submitted in partial fulfilment of the requirements for the
B.Sc. (Hons.) in Computer Engineering*

Copyright Notice

Copyright in text of this dissertation rests with the Author. Copies (by any process) either in full, or of extracts, may be made only in accordance with regulations held by the Library of the University of Malta. Details may be obtained from the Librarian. This page must form part of any such copies made. Further copies (by any process) made in accordance with such instructions may only be made with the permission (in writing) of the Author.

Ownership of the right over any original intellectual property which may be contained in or derived from this dissertation is vested in the University of Malta and may not be made available for use by third parties without the written permission of the University, which will prescribe the terms and conditions of any such agreement.

Plagiarism Declaration Form

FACULTY OF INFORMATION AND COMMUNICATION TECHNOLOGY

Declaration

Plagiarism is defined as "the unacknowledged use, as one's own, of work of another person, whether or not such work has been published, and as may be further elaborated in Faculty or University guidelines" (University Assessment Regulations, 2009, Regulation 39 (b)(i), University of Malta).

I / We*, the undersigned, declare that the [assignment / Assigned Practical Task report / Final Year Project report] submitted is my / our* work, except where acknowledged and referenced.

I / We* understand that the penalties for committing a breach of the regulations include loss of marks; cancellation of examination results; enforced suspension of studies; or expulsion from the degree programme.

Work submitted without this signed declaration will not be corrected, and will be given zero marks.

* Delete as appropriate.

(N. B. If the assignment is meant to be submitted anonymously, please sign this form and submit it to the Departmental Officer separately from the assignment).

John Napier

Student Name

Signature

Student Name

Signature

Student Name

Signature

Student Name

Signature

ICT3903
Course Code

Image Processing Techniques for Brain Haemorrhage
Detection in Head CT Scans
Title of work submitted

26/05/17
Date

Acknowledgements

My sincere thanks goes to my supervisor: Prof. Ing. Carl J. Debono as well as my co-supervisors: Dr. Paul Bezzina and Dr. Francis Zarb for their help and guidance throughout this study. They were always available and eager to provide help whenever I needed it and made this learning experience a positive one.

I would like to express immense gratitude towards family for always supporting me throughout my life. Without their constant hard work and encouragement I would have never made it this far into my studies. I would like to specifically thank my mother for always pushing me to achieve the best results and to aim as high as possible.

Last but not least a big thank you goes to my course mates, especially Matthew, Mark and Shaun for making this whole learning experience a positive one.

Abstract

Medical imaging is an important tool used for obtaining visual information of the interior of the body. There exist various imaging modalities such as Magnetic Resource Imaging, Ultrasound and Computed Tomography (CT). The latter is used extensively for detection and diagnosis of brain haemorrhage.

Computer Aided Detection/Diagnosis (CAD) systems are used by radiologists as a tool which helps them during the diagnosis phase. Increasingly, CAD is becoming a key component of routine clinical practice in several medical areas such as mammography and colonoscopy. Research regarding brain CAD systems has not progressed at the same pace as research in the mentioned areas. This provides a need as well as an opportunity to contribute to the research by developing a CAD system for brain haemorrhage detection and classification.

This study applies image processing techniques to brain CT scans with the aim of creating a CAD system which detects fresh bleeds. The system also includes a basic classification that identifies the haemorrhage type. The system distinguishes between an intra-axial haemorrhage and an extra-axial haemorrhage with the only limitation being subarachnoid haemorrhage (SAH), which is not always properly classified due to its complex structure. The techniques implemented in this study include noise reduction methods through the use of filters, morphological operations and segmentation algorithms, such as thresholding and clustering.

The designed CAD system was tested on 36 brain CT sets obtained from the general hospital in Malta. The results show that the system achieved a sensitivity of 94.4%, a specificity of 94.4%, a precision of 91.259% and a classification accuracy of 88.89%. The system performed the required operations in an average time of 0.26 seconds per slice.

Table of Contents

Copyright Notice	i
Plagiarism Declaration Form	ii
Acknowledgements	iii
Abstract	iv
Table of Contents	vi
List of Tables	vii
List of Figures	ix
List of Abbreviations	x
1 Introduction	1
1.1 Computer Aided Detection/Diagnosis in more detail	1
1.2 Computed Tomography	2
1.3 Focus of this Study	5
1.4 Structure of this Report	7
2 Literature Review	8
2.1 Noise Removal	8
2.2 Contrast Enhancement	13
2.3 Segmentation	16
3 Design & Implementation	26
3.1 Overview of the Implemented CAD System	26
3.2 Noise Removal	27
3.3 Segmentation	31
3.4 Detection	33
3.5 Classification	38
3.6 Output	39
4 Testing and Evaluation	41
4.1 Results	41

4.2	Comparison with other CAD Systems	44
4.3	Observations	45
5	Conclusion and Future Work	48
5.1	CAD System Overview and Conclusion	48
5.2	Future Work	49
	References	52
	Appendix	App. 1
(A)	A Whole Brain CT Scan Set	App. 1
(B)	Documents Pertaining to the Approval of use of CT Scans and Medical Reports from a General Hospital in Malta	App. 11

List of Tables

3.1	Gaussian filter parameter values tested	29
3.2	Median filter parameter values tested	29
3.3	Bilateral filter parameter values tested	31
3.4	Wiener filter parameter values tested	31
4.1	Comparison between the results obtained in this study, and those from other studies	45

List of Figures

1.1	Processes used in the scanning and data acquisition phase; (1.1a) A graphical representation of the x-ray beams, views and detectors [1], (1.1b) The spiral scanning process [1]	4
1.2	(1.2a) Factors determining radiation dose to the patient [1], (1.2b) Factors determining the image detail [1]	5
1.3	An example of brain haemorrhage, where the hemorrhagic region is highlighted in red [2]	6
2.1	Voxels in a CT image. [1]	9
2.2	Effect of the parameters chosen [1].	9
2.3	The reference image and the corresponding ROI [3]	18
2.4	Binarized Mask and Final Brain Candidate [3]	18
2.5	Topographic Interpretation when A Watershed Transform Is Applied To An Image [4]	19
2.6	a) original image, b) image after the skull and ventricles are removed, c) image after noise reduction, d) mask of the image, e) image after removing the soft tissue edema [5]	20
2.7	(a1) - (a3) Results of intensity rescaling; (b1)-(b3) Brain matter; (c1)-(c3) CSF after applied mathematical morphology [6]	21
2.8	Histogram showing the tissue peak, FWHM, and initial threshold for haemorrhage slice identification and haemorrhage region segmentation [7]	23
2.9	The Process of FCM Based Segmentation [7]	24
3.1	Flow Diagram of the CAD System implemented in this study	26
3.2	The Resulting images after filtering; (3.2a) original image, (3.2b) applying a Gaussian filer having a kernel size of 17, (3.2c) applying a Median filter having an aperture linear size of 9, (3.2d) using a Bilateral filter with a pixel neighbourhood diameter of 27, a colour standard deviation of 34 and coordinate space standard deviation of 13.5, (3.2e) using a Wiener filter with a constant of 0.7	30
3.3	The effect of the morphological operations on the image; (3.3a) Image after applying fixed-level threshold, (3.3b) Image after applying morphological operations	32
3.4	The removal of the skull and final brain segmentation; (3.4a) Image after removing any bones and applying erosion and dilation, (3.4b) Final segmented brain	34

3.5	Another example of segmenting the brain from the skull, however this time with less bone structures; (3.5a) Original unprocessed image, (3.5b) Image following segmentation processes	34
3.6	The result after applying fixed-level thresholding with the newly obtained lower and upper thresholds; (3.6a) Image following segmentation processes, (3.6b) Result obtained after applying fixed-level thresholding	36
3.7	An example of extra-axial haemorrhage [8]	38
3.8	Examples of the results obtained after successfully detecting haemorrhage	40
4.1	Typical output obtained from the CAD system	43
4.2	Last four image slices of the CT set seen in Figure (4.1)	44
4.3	An example of low contrast CT images of a brain which contains haemorrhage	46
4.4	An example of a false positive result which occurred due to the skull outline	46
4.5	An example of how the skull pixels can effect the shape of the contour . . .	47

List of Abbreviations

AHE Adaptive Histogram Equalisation

AI Artificial Intelligence

CAD Computer Aided Detection/Diagnosis

CDF Cumulative Distributive Function

CLAHE Contrast Limited Adaptive Histogram Equalisation

CSF Cerebrospinal Fluid

CT Computed Tomography

DFT Discrete Fourier Transform

DRLSE Distance Regularised Level Set Evolution

DWT Discrete Wavelet Transform

EDH Epidural Haemorrhage

EM Electromagnetic

EM Expectation Maximisation

FCM Fuzzy C-means

FMM Fast Marching Method

FOV Field of View

FWHM Full-Width Half-Maximum

GM Grey Matter

HE Histogram Equalisation

HKMDHE Hyper Kurtosis Based Modified Duo-Histogram Equalisation

HU Hounsfield Unit

ICH Intracerebral Haemorrhage

IVH Intraventricular haemorrhage

MDRLSE Modified Distance Regularised Level Set Evolution

MLSA Multi-level Local Segmentation Approach

MM Modified Mean

MSE Mean Square Error

NL-means Non-Local Means

PSNR Peak Signal-to-Noise Ratio

ROI Region of Interest

SAH Subarachnoid Haemorrhage

SAWM Switching-based Adaptive Weighted Mean

SDH Subdural Haemorrhage

TF Transform Function

WM White Matter

WMF Weighted Median Filter

1 Introduction

Brain haemorrhage is a leading cause of death of humans in the 15 to 24 age bracket, and is the third most common cause of death when considering all other age groups [5]. Detecting the correct location and type of brain haemorrhage is crucial in saving the lives of patients and preventing further damage. There are many causes for brain haemorrhage, with the two most common being trauma (most common cause of brain haemorrhage in the 15 to 24 age bracket) and stroke (most common cause of brain haemorrhage when considering all other age groups). Hemorrhagic stroke can be caused by a brain aneurysm burst or a weakened blood vessel leak. In each case, blood spills into or around the brain and creates swelling and pressure. This swelling and pressure consequently causes damage to the cells and tissue found inside the brain. Computed Tomography (CT) scans are the primary tool used for diagnostics in order to determine whether a patient needs surgery or not. When viewing a CT scan, intracerebral haemorrhage can be seen as a high density area which becomes less dense as time passes, eventually leaving a low density area [9]. The quality of the CT scan (which varies with patient positions and imaging artefacts) is vital for an accurate diagnosis. Reduced quality in CT scans can mean that small volumes of blood can be difficult to detect.

With the advent of image processing techniques, Computer Aided Detection/Diagnosis (CAD) has become increasingly more common in its use during routine clinical practice. CAD has been found to be extremely useful for decision support as well as in the detection and interpretation of various pathologies [10]. These systems therefore help medical personnel in their day to day work with the aim of preventing human error.

The aim of this study is to use image processing techniques to develop a CAD system which can detect the presence of haemorrhage in brain CT scans as well as provide a basic classification regarding the type of haemorrhage found. Therefore, this system can be used as a tool by radiologists and is in no way meant to replace the human aspect of brain haemorrhage detection and evaluation.

1.1 Computer Aided Detection/Diagnosis in more detail

CAD is becoming a vital component in medical practice, and it is used in order to help with the detection, interpretation, assessment and decision making in relation to medical imaging [10]. A CAD system uses image processing techniques to highlight a possible region of interest thereby offering input to support the decision which will be taken by the professional. CAD is therefore limited to being a supportive tool and is not intended in any way

to replace the professional. This means that the performance obtained from a CAD system does not need to be on the same level or surpass that of the physician, rather it needs to be complementary [11].

With the rapid increase in the number of medical images that need to be processed daily, there is a growing interest in CAD systems among radiologists [12]. As a consequence, CAD has become one of the major research subjects in medical imaging and diagnostic radiology, with most research being targeted towards chest, breast, and colon [11]. Many CAD systems have already been developed targeting many medical areas, with a large number being successfully adopted for use in early detection of breast cancers on mammograms [11].

Observer Performance studies performed by Feng Li *et al* [13] provide proof that CAD systems can have a positive impact on the diagnostic accuracy of radiologists. Radiologists using a CAD scheme for distinction between benign and malignant lung nodules demonstrated more confidence when diagnosing and their performance was better than that of their counterparts who did not have access to the CAD system. Through the use of these systems, the decision making process improved and the real benefit was seen when subtle cases were encountered. Another important finding was that incorrect or inaccurate computer output did not have a detrimental effect on the performance of radiologists as they were still able to apply and maintain their own judgement.

1.2 Computed Tomography

Computed tomography (CT) is an imaging procedure that makes use of x-ray equipment to create high-quality images of areas inside the body for diagnostic procedures [14]. These images can provide a view from multiple planes and can even be manipulated to provide a 3D view of the scanned body area. Although CT is a non-invasive technique, it exposes the patient's body to a relatively high dose of radiation. Imaging protocols affect both the image quality and radiation dose. These protocols are specific per patient and altered according to which anatomical structure needs to be viewed and at which quality in order to avoid exposing the patient to a radiation dose which is larger than is required.

1.2.1 CT Image Formation Process

Forming an image using CT is a three-stage process, each with its own adjustable protocol factors [1]. The first phase includes scanning and data acquisition where scan data is pro-

duced and stored on a computer. Image reconstruction is the second phase and this results in a series of sequential digital 2D image slices or a 3D volume. The third and final phase is that of converting the digital data into visible analogue images for viewing.

1.2.1.1 Scan and Data Acquisition

During the scanning phase, the scan beam performs two distinct motions relative to the patient's body. The x-ray tube and beam rotate around the width of the patient's body in order to obtain many 'views', whilst the other scanning motion takes place along the length of the patient's body. These two motions are combined to form a complete data set from where the required images can be reconstructed. An x-ray tube position usually projects a thin fan shaped beam through the patient's body and this is then intercepted by an array of radiation detectors. Views are obtained about every one degree of an angle so that every scan around the body produces a large number of views, usually in the hundreds. This high number of views is required and is indeed necessary to produce a high quality image for each slice. A graphical representation of the x-ray beams, views and detectors can be seen in Figure (1.1a).

The two main methods of scanning the beam along the length of the body are the 'scan and step' method, and spiral or helical scanning [1]. The latter is the most modern and preferred method and works by having a continuous rotation of the x-ray beam around the body with the concurrent movement of the body through the scanner. This means that the body area being scanned is not made up of individual slices but rather a continuous stream of data. This allows for slice thickness of the images to be determined at the reconstruction phase and not at the time of scanning and data collection, therefore allowing for reconstruction of different slice thickness without having to scan the patient multiple times. An illustrated representation of spiral scanning can be seen in Figure (1.1b).

1.2.1.2 Image Reconstruction

The data of the scanned anatomical area is transformed into the required digital image in this stage of the process. The main processes used to create these images are the filtered back-projection method and the enhanced process known as iterative reconstruction. Each slice is divided into a matrix of voxels as seen in Figure (2.1). The size of individual voxels critically effects the CT image quality and is controlled through protocol factors such as Field of View (FOV), matrix size and slice thickness [1].

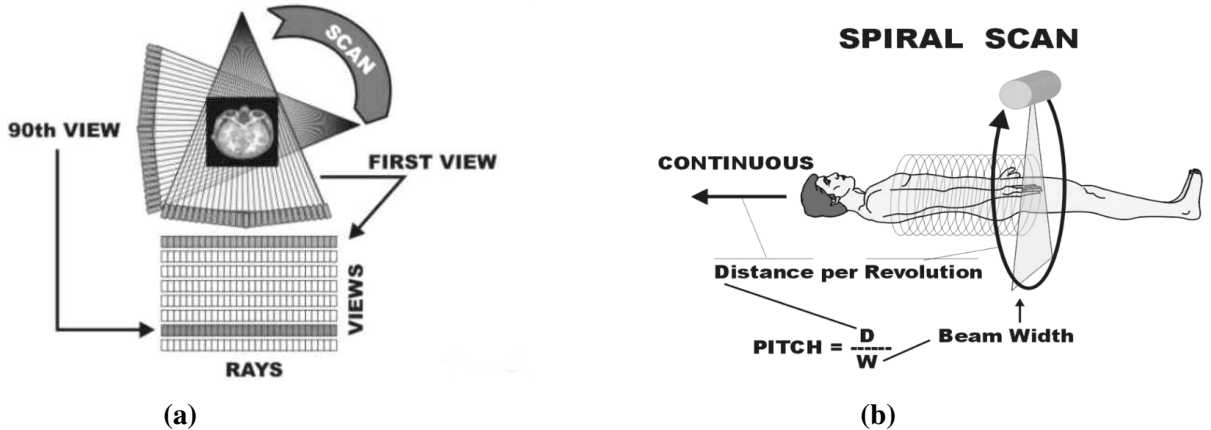


Figure 1.1: Processes used in the scanning and data acquisition phase; (1.1a) A graphical representation of the x-ray beams, views and detectors [1], (1.1b) The spiral scanning process [1]

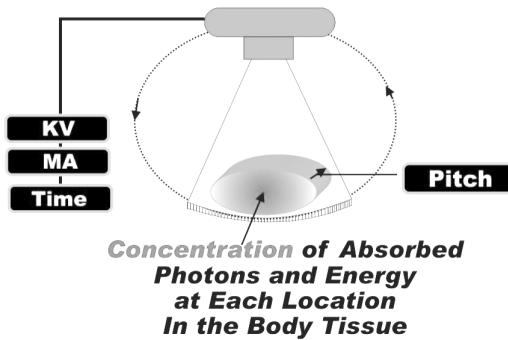
1.2.2 Radiation Dose

An important factor in CT image quality and patient health is radiation dose. The propagation of energy through simultaneous vibration of electric and magnetic fields is known as Electromagnetic (EM) radiation. X-rays are part of the EM spectrum and are created when electrons are accelerated to energies greater than 5 kV and then directed onto a target surface [15]. At energies chosen for diagnostic radiology, some of the x-rays are absorbed by tissue. When dealing with medical imaging, the main densities that need to be considered are gas, fat, soft tissues and calcified structures [9]. X-rays passing through gas are the least absorbed, and so they cause the most blackening on the radiograph, whereas rays that pass through bone structure appear white as calcium absorbs the most. Most soft tissues have the same absorptive capacity and therefore appear the same shade of grey. However, CT expands the number possible densities to more than 2,000 shades of grey, allowing for distinction between various soft tissues [9].

When dealing with radiation dose to patients, there is a small risk that the absorption of x-rays can induce cancer or genetical mutations that lead to genetical diseases in offspring [16]. The risk of developing the mentioned pathologies is very much dependent on various factors which include the part of the body exposed, the patients age and the patients gender. It is generally assumed that the risk of adverse health effects from cancer is proportional to the amount of radiation absorbed and that there is always a risk when dealing with radiation exposure.

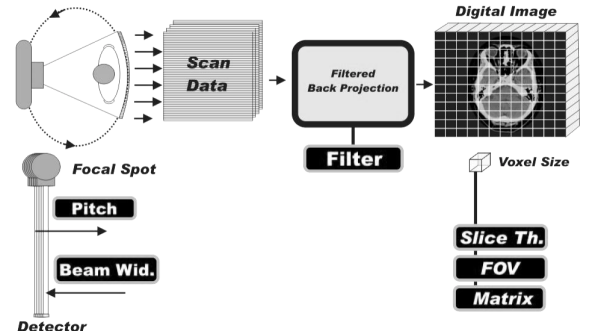
Although possibly having an adverse health effect, radiation dose is instrumental to improv-

Factors That Determine Radiation Dose to Patient



(a)

Factors That Determine Image Detail (Sources of Blurring)



(b)

Figure 1.2: (1.2a) Factors determining radiation dose to the patient [1], (1.2b) Factors determining the image detail [1]

ing the image quality. The dose is dependent on the anatomical structure location being analysed as well as protocols such as tube voltage (kV), current-time product (mAs), pitch and time of exposure. An ideal protocol is considered one in which the selected factors are chosen in order to obtain a balance between dose and image quality.

1.2.3 Factors Affecting Image Detail

The majority of the blurring that is seen in a CT image occurs during the scanning and reconstruction phases. The x-ray beam used during the scanning phase is divided into many small rays. The size of the individual rays is determined by both the focal spot of the scanner and the size of the detector. For good image detail, it is important that small rays are used [1]. Another factor to be considered is the pitch and the focal spot. Increasing the pitch causes a spreading of the ray leading to blurring along the length of the body. This means that for an image containing high detail, scanning needs to be performed with a thin beam and low pitch value. Additional causes of blurring are the mathematical filter in the reconstruction calculation and the size of the tissue voxel. Figure (1.2b) provides an illustrated representation of the factors that cause image blurring.

1.3 Focus of this Study

This study focuses on creating software capable of detecting and classifying haemorrhage (fresh bleed) found in the brain. The classifier will classify the haemorrhage as being intra-axial or extra-axial, with the only limitation being when classifying subarachnoid haemorrhage (SAH). This limitation occurs since the SAH haemorrhage shape and location differ

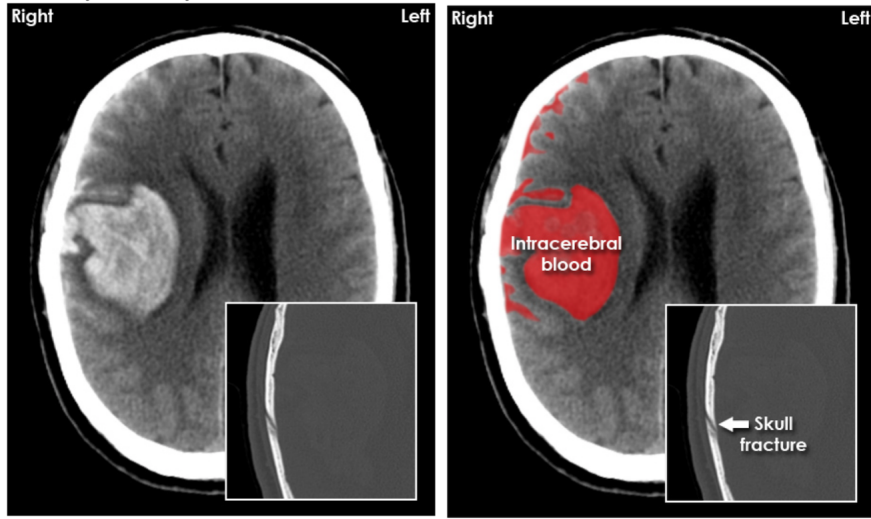


Figure 1.3: An example of brain haemorrhage, where the hemorrhagic region is highlighted in red [2]

vastly from the rest of the haemorrhages in the extra-axial group. The brain is a highly important complex organ as it serves as the centre of the nervous system and controls most of the activities of the body [17]. Haemorrhage can be defined as blood escaping from the circulatory system [18] and can occur internally as well as externally.

When analysing brain CT scans with haemorrhage, it can be noted that the hemorrhagic region forms a white hyper-dense area compared to the rest of the brain. This means that regions belonging to the haemorrhage appear to have a whiter intensity when compared with the rest of the brain which appears to be darker. Another characteristic of brain haemorrhage is that it can be seen to be present in multiple CT slices. The volume of blood can be seen to change throughout the slices as it first appears to be small, then it gradually increases before decreasing again and eventually disappearing. An example of a typical case of brain haemorrhage can be seen in Figure (1.3) and an entire CT set of a brain in which haemorrhage is present is found in Appendix A.

The aims of this study are the following:

- Applying image processing techniques on CT scans to detect the presence of haemorrhage (fresh bleed) in the brain.
- Developing an algorithm to enclose and highlight the detected region.
- Developing a method for basic classification of the detected haemorrhage type.

- Evaluating the accuracy of the detection and classification algorithms and compare the results to published work.
- Proposing any improvements that can be applied to the developed CAD system.

Literature concerning CAD systems for brain haemorrhage detection is not as vast as that of other areas. Therefore, the development of a CAD system as proposed in this study will be of great benefit to radiologists and patients alike and can lead to future research and developments in this area.

1.4 Structure of this Report

This report is structured as follows:

- Chapter 2 contains a literature review explaining the processes and techniques which are at the core of this project as well as the current literature available in these areas.
- Chapter 3 provides a detailed explanation of the design and implementation of the CAD system discussed in this study.
- Chapter 4 discusses the results of the experiments conducted and compares them with existing CAD systems in order to gauge the effectiveness of the system.
- Chapter 5 contains a summary of the study and also discusses the possibility of any room for future improvement of the system.

2 Literature Review

This section addresses background techniques applied in CAD system development and other similar applications. These techniques mainly include noise removal, contrast enhancement, and also segmentation. To tackle this particular problem the literature pertaining to these procedures will be compared and analysed.

2.1 Noise Removal

The presence of artefacts and noise in CT images can greatly increase the difficulty of medical diagnosis[19]. A combination of protocol factors may be used to adjust noise in a CT image. The noise present in CT images is a form of quantum noise and this is caused by the natural random distribution of the photons over the image area [1].

As seen in Figure (2.1), a CT image is composed of a large voxels. The size of these voxels has a great effect on noise, image blurring, as well as on the radiation dose the patient is exposed to. Noise is caused by the resulting statistical errors obtained from measuring the CT numbers of each tissue voxel. When reconstructing images, small voxels lead to reduced blurring and better image detail. On the other hand larger voxel sizes reduce noise as more photons are captured [1].

Noise and statistical error may be reduced by increasing the X-ray dose to the detriment of the patient[20]. The dose is controlled by the tube voltage (measured in kV), the current-time product (mA) and pitch [1]. The values of these parameters are changed in order to increase the image detail and reduce the noise level. Figure (2.2) shows how these have an effect on a CT image. For example, when thin image slices are needed in order to increase the image detail, the mA needs to be automatically increased in order to maintain a specific noise ratio. Therefore the selection of the mA is crucial as it has a direct effect on the x-ray dose as well as noise. The mA, kV and pitch values are altered according to the individual body size, shape and composition [1].

During the image reconstruction phase, the mathematical filter used has an effect on the noise and image detail. Different filters may be chosen so as to reduce the amount of noise in an image. This in turn reduces or increases the image detail [1]. When selecting a reconstruction filter, consideration has to be given to the balance between the image detail and the amount of noise present in the image.

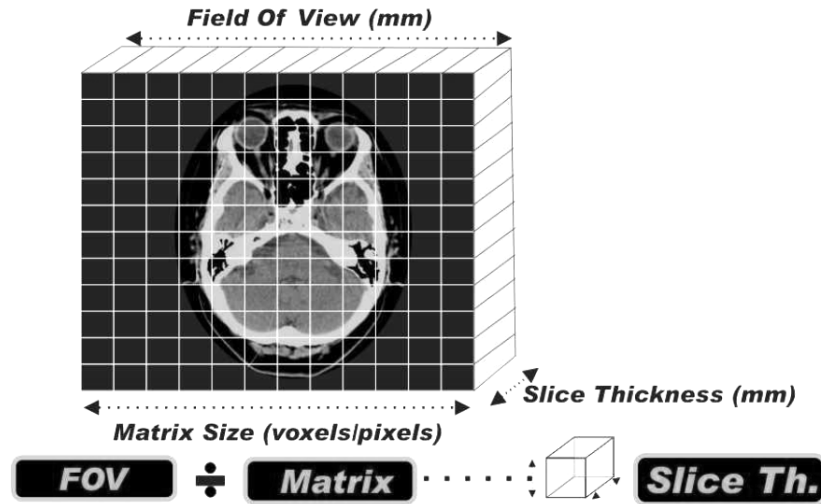


Figure 2.1: Voxels in a CT image. [1]

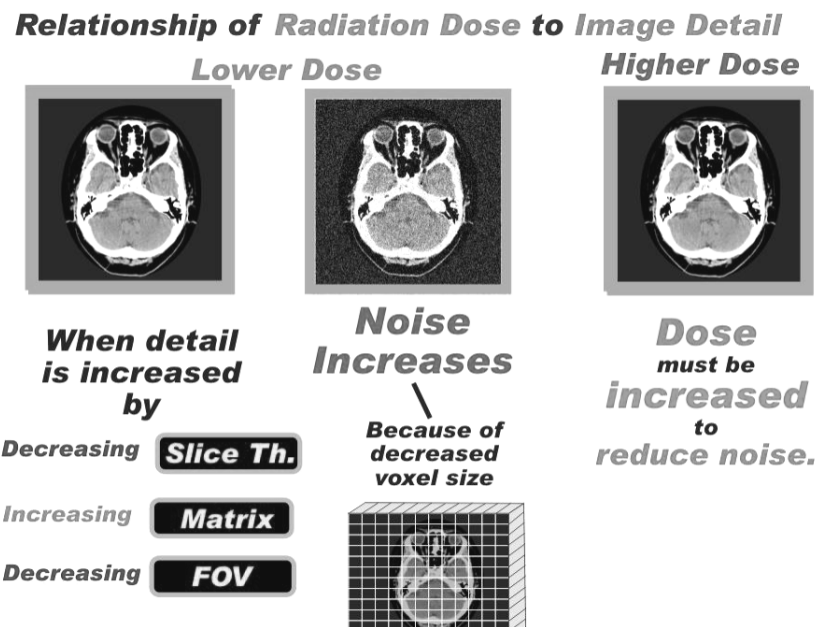


Figure 2.2: Effect of the parameters chosen [1].

The reduction of the radiation exposure by a factor of 2 leads to an increase in noise by approximately a factor of $\sqrt{2}$. This in effect means that the ratio between relevant tissue contrasts and the amplitude of noise must be adequately large for a dependable diagnosis[21]. Therefore in order to bring about an improvement in image quality, noise reduction techniques are used with the aim of using lower dose images whilst still preserving all medically relevant structures. Noise Filtering is one of the first pre-processing steps applied before supplying a CAD system with a CT image.

Chhabra *et al* [22] explain how most denoising algorithms incorrectly assume additive white Gaussian noise, when in fact, most medical images may contain different types of noise such as Poisson noise. The authors compare anisotropic diffusion, Wiener filtering, anisotropic diffusion in wavelet domain, wavelet decomposition, wave atom decomposition, non-local means (NL-means) filtering and median filtering.

The **Median Filter** is a type of non-linear filter. In this filter, the values (based on intensity or brightness level) of the neighbouring pixels are used to determine the value of the pixel under evaluation. This value is calculated by taking the median value of the surrounding pixel values [22]. The median filter is effective to de-noise images effected by shot or impulse noise. There are several advantages enjoyed when using the median filter over other smoothening filters [23]. These advantages include no reduction in contrast, no shifting in boundaries and minimum degrading of edges. A modified median filter is the **Weighted Median Filter (WMF)**. This filter provides a way of removing unwanted content while providing the facility to preserve the desired features of the image and therefore the WMF can be designed to work in a controlled manner [24].

A different filtering technique is **Wavelet Decomposition**. The wavelet transform is a mathematical technique used for synthesis of signals in the time domain. An unknown signal can be analysed by combining it with the wavelet transform and the data variables are analysed both in the time and frequency domain. In Discrete Wavelet Transform (DWT), the signal is decomposed into several levels which are analysed independently [22]. This signal decomposition is performed through the use of orthogonal wavelets and can be shown by the following equation:

$$s(l) = \sum_k C_{j,k} \phi_{J,I}(k) + \sum_{j=i}^k W_{j,k} \psi_{j,k}(k) \quad (2.1)$$

where, $\psi_{j,k}(x) = 2^{-j}\psi(2^jx - l)$ and $\phi_{j,k}(x) = 2^{-j}\phi(2^{-j}x - l)$. A threshold (in the form of either a hard threshold or a soft threshold) is applied to wavelet coefficients in order to

achieve noise reduction. Wavelet functions which are commonly used include the symmlet, haar, coiflet and daubechies [22]. The selection of which wavelets to use is done by taking into consideration the wavelet shape as well as their ability to analyse the signal in a particular application.

Another filter that can be used to reduce noise is the **Wiener Filter**. This filter is considered as the optimal linear filter and is ideal for filtering blurred images and images which contain additive noise [25]. The optimisation problem of this particular filter is to minimise the Mean Square Error (MSE) value. This is the difference between the required output and the obtained output. This filter only works well if the underlying signal is smooth [25] due to the fact that when the input is non stationary, the optimum filter will need to assume a time varying form [22]. If for example the chosen filter is $G(u, v)$, then the resultant image is given by:

$$X(u, v) = G(u, v) \times Y(u, v) \quad (2.2)$$

where $G(u, v)$ is chosen so that the mean squared error is minimised [26].

Another family of filters is the **Mean Filter**. This filter is also known as the average filter and it is considered to be a windowed filter of linear class which can be used to smoothen images and to reduce noise [25]. This filter works similarly to the median filter since it operates by using the neighbours of an element in consideration. The sum of the pixel intensities of the neighbouring pixels is computed and divided by the number of neighbours. The pixel value in consideration is then replaced by the computed average [25]. According to Zhang *et al* [27], the standard median filter tends to damage vital details such as thin lines and corners. The authors explain that although alterations to the median filter (such as the weighted median filter) have been proposed, these alterations are still implemented for all the pixels in the image and they therefore cause the modification of the untouched good pixels. The authors therefore recommend the **switching-based adaptive weighted mean (SAWM) filter**, which is a modified mean filter which aims to remove salt-and-pepper noise. This filter makes use of a directional difference based noise detector combined with an adaptive weighted mean filter to restore the noisy images. Through testing, the authors concluded that the proposed filter is more effective in identifying salt-and-pepper noise and provides better image restoration performance than the median filters mentioned.

Borsdorf *et al* [21] introduce a new wavelet based structure-preserving method which can be used in the reduction of noise in CT-images in combination with different reconstruction methods. The approach makes use of the assumption that data can be broken down into

information and temporally uncorrelated noise. In CT, two spatially identical images can be produced by using disjoint subsets of projections for reconstructions. This can be done by making use of dual source CT-scanners where the first image can be generated from the projections obtained from the first detector, and the second image acquired from projections obtained from the second detector. In the case of standard CT-scanners, the set of projections can be split into even and odd numbered projections so as to obtain the same two images obtained using the dual source CT-scanners. The images resulting from this process show mostly the same information but contain differences in image noise:

$$\text{Image } A = S + N_A \quad \text{AND} \quad \text{Image } B = S + N_B \quad (2.3)$$

where S is the common signal and N_A, N_B are the respective noise signals. The analysis of correlations between the input image wavelets allows for the separation of valid information from noise down to a required signal-to-noise level. Wavelet coefficients with small correlation are suppressed, whilst the rest are presumed to represent structures and are preserved. The final image with reduced noise is obtained from the averaged and weighted wavelet coefficients of the input images. This method is reliable, simple and is able to adjust itself to the noise present in the particular images.

Anisotropic Diffusion is an alternate approach which can be taken to reduce noise in images. Chhabra *et al* [22] compare diffusion filtering of an image to the physical diffusion process as in both cases an equilibrium is obtained. The authors explain that the image intensities are seen as a ‘concentration’ whereas the noise can be seen as noise inhomogeneities which can be evened out by ‘diffusion’. There are two types of diffusion filtering in image processing - *linear* and *nonlinear* diffusion. Linear diffusion is used in order to smoothen an image. However, it tends to blur features such as edges. In nonlinear diffusion the filter coefficients are altered in direct response to differential structures within an image [28]. On the other hand, a different form of anisotropic diffusion is **Anisotropic Diffusion in Wavelet Domain**. Chhabra *et al* [22] explain that various wavelet shrinkage algorithms de-noise an image by reducing the wavelet coefficients and by making use of statistical information pertaining to wavelet coefficients. Furthermore, image anisotropic diffusion uses neighbouring information and adjusts diffusion conductivity by edge magnitude. It follows that Anisotropic Diffusion in the wavelet domain combines these two in order to produce better results.

2.2 Contrast Enhancement

Contrast enhancement is another pre-processing step used in CAD systems. This step is used so as to be able to distinguish between various objects found in an image as well as to aid in fully understanding the information being provided by the image [25]. In CT imaging, the window setting allows for the visualisation of CT brain images. However, the standard window setting for CT brain images fails to produce a contrast which is good enough to attenuate the hypo-dense area in the brain soft tissues [29], further highlighting the need for this technique.

An image histogram consists of all the pixel intensity values. For 8-bit grayscale images there are 256 different possible intensities, meaning that the histogram will consist of 256 numbers which represent the distribution of the pixels amongst those grayscale values. A popular contrast enhancing method is **Histogram Equalisation** (HE). The HE method uses the image cumulative distributive function (CDF) to derive a nonlinear transform function (TF). This is in turn used to reassign grey scale values to new values [29]. Considering that an image is expressed as a set of data, where the grey level X has the range of $[0, 255]$ and where the CDF is X_k , the TF is derived from:

$$TF = (X_{max} - X_{min})c(X_k) + X_{min} \quad (2.4)$$

where X_{max} and X_{min} are the maximum and minimum grey level in the output image [29]. According to Tan *et al* [29], the conventional HE method stretches the levels with high probability more than levels with low probability. Therefore this results in an over enhancement in the background of the image since the background levels have a higher distribution.

Adaptive Histogram Equalisation (AHE) works in a similar way to the conventional HE method. However, several histograms are computed for each image which correspond to distinct image sections. These are then used to redistribute the brightness value of the image, greatly improving the perception of the image [25]. A drawback of this method is usually high computational complexity and the fact that it is sometimes prone to block related artefacts [30]. **Contrast Limited Adaptive Histogram Equalisation** (CLAHE) is much more efficient as it operates on small sections (tiles) of the image rather than on the whole image. These sections are then combined using bilinear interpolation to avoid an artefact [31].

Another technique is **contrast stretching**. This technique attempts to improve the contrast of an image by stretching the range of intensity values to span a desired range of values. A

linear mapping of the input to the output values is then performed. The first step in contrast stretching is to determine the upper and lower pixel value limits over which the image is going to be stretched. Usually these limits are the maximum and minimum values that the image type in question allows (grey scale 0 - 255), or they can also be determined from the image histogram [25]. The original value in the image is mapped onto the value in the output image using the following equation:

$$Output = (Input - c) \left(\frac{b - a}{d - c} \right) + a \quad (2.5)$$

where:

- a and b are the lower and upper limits
- c and d are the lowest and highest pixel values currently present in the image.

The three contrast enhancing techniques mentioned above (HE, AHE and Contrast Stretching) are discussed and compared by Malik *et al* [25]. The authors note that when taking visual inspection into consideration, AHE is much more effective in enhancing the contrast as well as preserving the details of a CT image and therefore produces better visual results when compared to HE and contrast stretching. On the other hand, according to image quality measuring techniques, contrast stretching outperforms other techniques as far as Peak Signal-to-Noise Ratio, Mean Squared Error, Root-MSE, Universal Image Quality Index and Pearson correlation coefficient are concerned.

Zhang *et al* [30] build on the AHE technique by proposing a contrast enhancement algorithm based on AHE which can be applied to low-dose CT images. The main idea behind the algorithm is to use local contrast-stretching manipulation in each sub-block of the image and then recompute the intensity of each pixel by making use of global and local image statistics. Each pixel is assigned a new intensity which is determined through an adaptive transfer function (TF). The design of this TF is based on the global and local statistics of the input image. The proposed contrast enhancement technique performs histogram equalisation based on a local modified contrast-stretching manipulation and replaces the intensity value of each pixel of the sub-block being taken into consideration. By applying their algorithm, the authors noted that the contrast considered as noise is reduced thereby reducing image noise and enhancing the features of the image. Through testing, it was shown that this method for contrast enhancement proved to be fast, could adaptively make tiny anatomies stand out more clearly as well as be affective in confining noise.

A different approach of enhancing contrast in CT images is that of making use of the un-sharp mask filter [32]. The first step in this method is to determine a region of interest (ROI). This is done through the generation of a binary mask, where pixels forming part of the ROI are set to white and the rest are set to black. Following the extraction of the ROI, the boundary of the ROI is marked by making use of a level set function. Contrast enhancement techniques are then used to further enhance the contrast of the image. The authors discuss two main categories of contrast enhancing techniques, namely linear, and non-linear techniques. The linear techniques work by performing linear stretching on the values of the pixels pertaining to the image. Different kinds of linear techniques include **Min-Max** linear contrast stretch, **piecewise linear** stretch, and **percentage** linear contrast stretch. Non-linear contrast enhancement commonly make use of histogram equalisations through the use of algorithms. The main disadvantage with the non-linear contrast stretch method is the fact that each and every value in the input image can have more than one value in the output image, implying that objects forming part of the original scene could end up with an incorrect relative brightness value [33]. Different kinds of linear techniques include **HE**, **AHE**, **CLAHE**, **un-sharp mask** and **homomorphic filters**. An un-sharp mask filter is used in the study in order to enhance the contrast the image. This filter increases the sharpness in the image contrast [33] and can be expressed by:

$$y(m, n) = f(m, n)a * g(m, n) \quad (2.6)$$

where f is the input image, y is the sharpened image, g is the gradient image and a is the contrast constant which is always greater than zero. Therefore, the sharpness of edges and other components in the image that have high frequency are improved by deducting the un-sharp version of an image from input image. The obtained image is then superimposed on the original image so as to achieve the ultimate result.

The **Hyper Kurtosis Based Modified Duo-Histogram Equalisation** (HKMDHE) algorithm proposed by Mukhopadhyay *et al* [31] makes use of **Hyper-Kurtosis** (β) and the **Modified Mean** (MM) so as to obtain contrast enhancement. Kurtosis provides the peak width and tail weight of a distribution, whereas hyper kurtosis (β) is used to provide the comparison with the normal distribution. In hyper kurtosis (β) the Power Law Transformation of mean (m) is implemented since the low contrast components in images are located near the mean. By applying this, the histogram of the original input image can be separated. The authors first make use of hyper-kurtosis (β) so as to improve the image contrast whilst still maintaining the image brightness. Then the modified mean (MM) is obtained by

calculating the square-root of the sum of the mean and hyper kurtosis. This specific point can be used to split input image histogram into two parts. The HE technique is then applied separately to both parts. The two separate parts are again joined resulting in an output image having much better contrast.

2.3 Segmentation

Image segmentation is a vital procedure in medical image analysis since it contributes to the basis of quantitative analysis of images associated with human pathology and functions. The manual segmentation of the entire set of images found in a medical database is a tedious and slow process. It follows that a procedure that automates segmentation is highly desirable [4]. Creating a segmentation technique is a difficult task since the images being processed are complex, there is a lack of anatomical models that capture all the structure deformities which have occurred, the presence of a low signal-to-noise ratio and the presence of artefacts present on many CT images [7].

When it comes to segmentation of haemorrhage in brain CT scans, many difficulties are encountered. This is due to various reasons such as the variability in the Hounsfield Units (HU) within the hemorrhagic region, partial volumes at the edges and the reasons mentioned above such as artefacts and noise [34]. Coupled with this, research regarding the segmentation of the brain from CT images is not as rich as that of segmentation from MRI data [3].

Prakash *et al* [7] explain that techniques associated with image segmentation can be mainly classified into 4 classes. These are **threshold-based**, **region-oriented**, **graph theory-based**, and **clustering methods**. The authors explain that the threshold-based technique is very intuitive and simple. The threshold is selected by taking features such as intensity, shape and size into consideration. Background information directly related to the feature on which the data is being classified is essential for this method. The majority of thresholding techniques perform binarization of the image so as to obtain foreground and background objects. Pixels which lie within a specified intensity range are grouped together and classified as the foreground object, whereas the pixels which do not lie within the specified intensity range are grouped into a second group and are classified as the background object. A limitation of this method is that an optimal threshold needs to be found in order to segment all the required objects.

Clustering techniques are ideal when the amount of classes in which the data has to be classified into is known and concurrently, there is not enough information regarding feature

values [7]. This technique is a form of unsupervised learning. Observations are assigned to clusters so as to group together similar observations. The **Fuzzy C-means** method is a commonly used fuzzy clustering technique used for solving multi class and unclear clustering problems and is also used in medical image segmentation.

Regarding the graph-theory based method, both local and global features are used for the classification of data. This is due to the fact that the derived graph of an image or data is dependent on the spatial relation (which is a local property) as well as other properties namely intensity and texture energy (which are global properties). Image segmentation is performed by partitioning image elements such as pixels into different regions [7]. All the pixels are then used to construct the graph and through various graph cut techniques, segmentation is obtained. The main constraint when using this method is the difficulty in choosing the right number of subsets since the image can be partitioned into many different amounts of subsets.

2.3.1 Skull Stripping

This is the process of extracting the human brain (consisting of grey matter (GM) and white matter (WM)) from the CT head volume. In CT brain images, bones have the highest intensity, followed by GM, WM, Cerebrospinal Fluid (CSF), and air [3]. Hu *et al* [3] implement a threshold-based method in order to segment the brain from the head. The authors explain that the first step is that of choosing a 2D reference image which well represents the original 3D volumetric CT data set. Therefore, the reference image ideally should contain WM, GM, CSF, air, and skull tissues. Next to be determined is a ROI known as the head mask - in this particular case it is the region found within skull. This is done by using Fuzzy C-means (FCM) clustering as well as the intensity histogram of the volume to classify the intensity into 4 clusters, with the smallest intensity being placed in the first group. The volume is then binarized by setting anything smaller than the maximum intensity of the first cluster plus 5 to 0 (background), and everything else to 1 (foreground). The authors then explain that the largest foreground connected object is then found and any remaining foreground objects are set to background. Any holes within the largest connected component are changed from 0 to 1 in order to obtain the finished head mask of which an example can be seen in Figure (2.3).

To remove air and CSF from the brain, the low and high thresholds within the ROI are determined next. The high threshold allows for the removal of bone that tends to be made up of higher pixel intensities than both GM and WM. Binarization is then performed on the

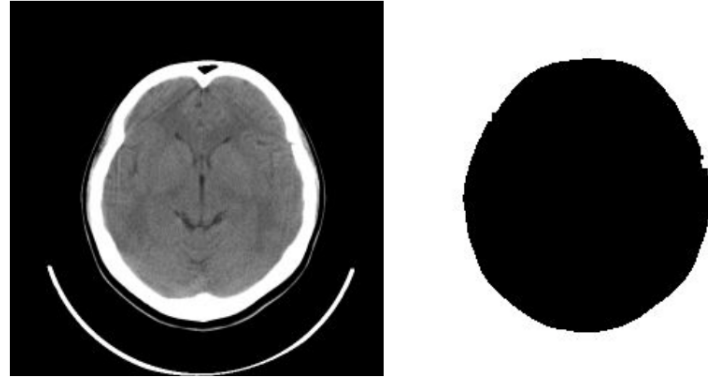


Figure 2.3: The reference image and the corresponding ROI [3]

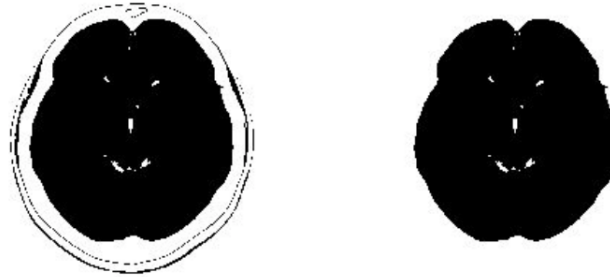


Figure 2.4: Binarized Mask and Final Brain Candidate [3]

original CT volume to get the binary mask using the following condition:

$$\text{BinaryMask} = \begin{cases} 1 & \text{Low Threshold} \leq \text{Original Volume} \leq \text{High Threshold} \\ 0 & \text{Otherwise} \end{cases}$$

The tissues and structures which do not belong to the brain are removed via brain mask propagation. Once this is done, the remaining brain candidate is the brain. Examples of the binary mask and the final brain candidate can be seen in Figure (2.4).

A different brain segmentation method that can be considered is **Watershed Segmentation** [4]. Watershed is a segmentation operator derived from the field of mathematical morphology. This segmentation method transforms the gradient magnitude of feature pixels' intensities with the aim of obtaining a topographic surface. The latter can be seen in Figure (2.5). The image is made to consist of *catchment basins* and *watershed lines*. This is done so that when the image is flooded from its minima, the waters from different 'lakes' do not merge. A disadvantage of this transform is the fact that in many cases over-segmentation is achieved as a result of noise or local irregularities in the gradient image. This can be solved

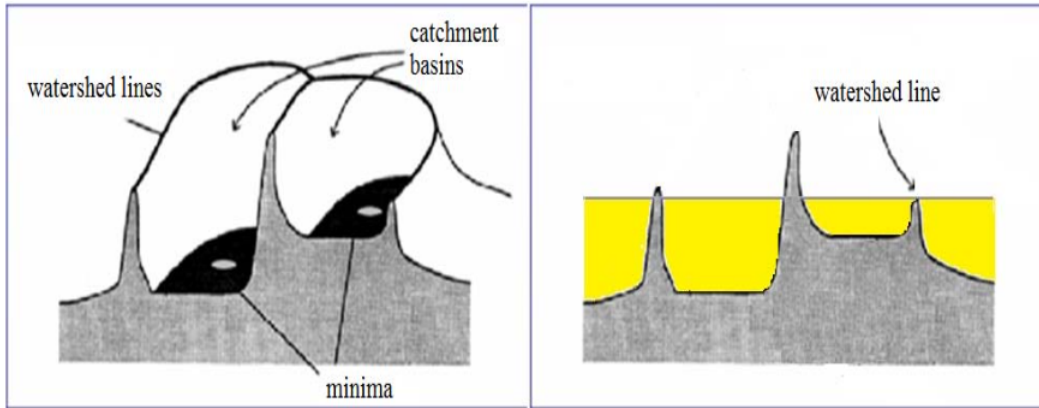


Figure 2.5: Topographic Interpretation when A Watershed Transform Is Applied To An Image [4]

by introducing **marker-controlled watershed**, which is a watershed transformation where the topographic surface can only be flooded from distinct marker locations. This method therefore avoids over-segmentation.

When the **Expectation Maximisation (EM) Method** is used for image segmentation, pixels are partitioned into clusters. This is achieved by calculating the maximum likelihood parameters of various established distributions when unobserved or hidden data is present. Although prior knowledge is incorporated into the algorithm, it is still an unsupervised segmentation method and hence no training is needed [35]. The data in the EM clustering approach is taken as a set of unlabelled samples which are then grouped. The grouping is based on similarity criteria. Each iteration of the EM algorithm involves an expectation step and a maximisation step.

Zaki *et al* [4] propose the **Multi-level Local Segmentation Approach (MLSA)**. This method involves using FCM clustering so as to extract the skull and ROI, followed by a second level of intracranial segmentation. In this second level the two-level multi-thresholding technique which is derived from the Otsu multi-thresholding concept [36] is applied. The authors compare this method to the EM method and the marker-controlled watershed method. The outcome of this comparison is that the MLSA method is superior to both compared methods due to it being simple and computationally tolerable, whilst still providing satisfactory results.

A simple method to successfully strip the skull, brain ventricles and soft tissue edema in brain CT images is used by Shahangian *et al* [5]. The authors explain that in the histogram

of a 2D CT brain volume, 3 peaks exist. The initial peak is formed as a result of the ventricles of the brain, the second peak is due to the brain itself (the object of interest), whilst the third peak (highest intensity) is formed as a result of the skull. The skull and brain ventricles are eliminated by changing the intensities of pixels having a value above 225 and below 100 in a grey scale map to 0. The next step is to remove any remnants of the skull that have not been removed. This is performed using image intensity adjustment and a median filter. In some images, soft tissue edema is present outside the skull. This is removed by making a mask which consists of the part of the image containing largest area, and then multiplying this mask with the image obtained from the previous step so as to remove the additional part (which becomes 0). These steps can be viewed in Figure (2.6).

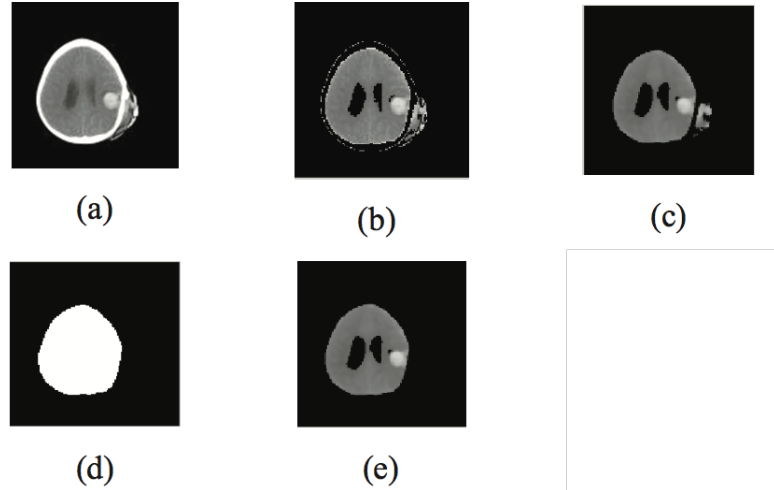


Figure 2.6: a) original image, b) image after the skull and ventricles are removed, c) image after noise reduction, d) mask of the image, e) image after removing the soft tissue edema [5]

To achieve segmentation, Zang *et al* [6] use a combination of intensity rescaling, the threshold algorithm, region growing method, fast marching method (FMM) and mathematical morphology. Intensity rescaling is performed since the range of intensities of the region of interest is small. Intensity rescaling is performed by obtaining the histogram of original images in order to determine the lower and upper limits, followed by transforming the intensities according to these limits through the use of a linear transformation function. After the images have been enhanced, the intracranial area is extracted using a threshold algorithm by setting the values of pixels which form part of the skull and background to zero. The intracranial area can also be extracted using the region growing algorithm as the skull consists of the largest connected component of the brightest areas in the images. Therefore, the region growing method can be implemented with the aim of obtaining and keeping largest connected component and discarding any other smaller connected components. FMM is a

special situation of level set method and is next used in order to segment the CSF and brain matter. Mathematical Morphology operations are used to fill the little holes in the CSF image. The two morphology operations used are dilation and erosion. The dilation operation expands the contour of the target object to fill the holes produced during the segmentation step. The Erosion is used to shrink the contour of the target object. The results of these processing steps can be seen in Figure (2.7).

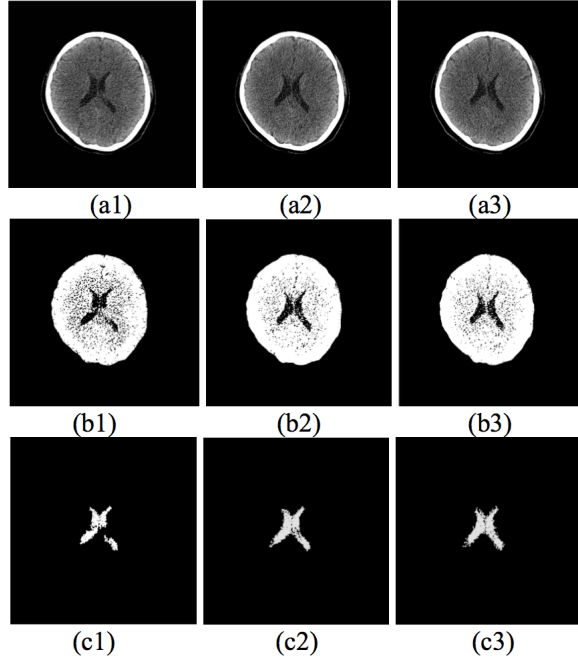


Figure 2.7: (a1) - (a3) Results of intensity rescaling; (b1)-(b3) Brain matter; (c1)-(c3) CSF after applied mathematical morphology [6]

2.3.2 Haemorrhage detection and Segmentation

When the above mentioned steps have been concluded, the haemorrhage detection and segmentation phase can commence. The success rate of this phase increases and indeed depends on the outcome of previous stages. In general, brain haemorrhages are classified into 5 main types: Epidural Haemorrhage (EDH) - Subdural Haemorrhage (SDH) - Subarachnoid Haemorrhage (SAH) - Intracerebral Haemorrhage (ICH) - Intraventricular Haemorrhage (IVH). Brain haemorrhage detection and classification is very helpful to professionals and enables them to treat patients at an early stage [5] and is essential for treatment planning. A good number of image segmentation algorithms are available in literature but very few studies on segmentation of haemorrhage have been conducted [34]. Factors such as the X-ray dosage, tissue contrast, intensity inhomogeneity, and irregular boundaries cause serious difficulties in the successful detection of haemorrhage from brain CT images [37].

Prakash *et al* [34] introduce a **modified distance regularised level set evolution** (MDRLSE) algorithm for haemorrhage segmentation. The distance regularised level set evolution (DRLSE) is a form of level set evolution without re-initialisation [38]. The authors note that the original DRLSE algorithm was able to successfully identify the strong edges in the scan but had difficulties in tracking the weak edges. Other limitations of this algorithm included the computational time, the influence of the initial position on the convergence as well as the number of iterations needed for convergence. Therefore the authors proposed a modified DRLSE algorithm to overcome these limitations by performing segmentation on two stages: shrinking and expansion. Shrinking was used to let the zero level contours surround the hemorrhagic regions rapidly. Properties such as the HU of blood (60-80) were used to identify the region. The authors assumed that the hemorrhagic area was made up of at least 20 pixels so as to reduce the occurrence of false positives. If at the end of the shrinking stage the difference between the area of the contour of the current iteration and the area of the contour of the previous iteration is negligible (less than a predefined threshold), then the algorithm terminates and proceeds to the next stage, otherwise it iterates further. During the expansion stage, edge information is used to expand zero level contours until the boundaries of the bright hemorrhagic regions are reached. This process was designed to expand through hemorrhagic regions and converge to the edges without surpassing them. The same area check was performed after each expansion iteration until the difference between the current area and the previous area is negligible. After segmentation, post processing is performed in order to remove as many as possible false-positive regions which were introduced due to over segmentation as well as remove false-negative regions caused by under segmentation. False-negatives were removed using automatic region growing. The authors state that MDRLSE is an improvement over DRLSE due to the algorithm being faster. This was achieved through a reduction in the number of iterative steps and by improving the accuracy through the use of anatomical and radiological information in pre-processing, segmentation and post-processing.

According to Prakash *et al* [7] the threshold, FCM, and the NCut methods can all be considered as valid methods for the segmentation of intraventricular haemorrhage (IVH) and intracerebral haemorrhage (ICH). When using the **modified threshold method**, haemorrhage segmentation is carried out slice by slice to take into consideration the variability of blood attenuation in each slice. A histogram of the brain including the haemorrhage regions of each slice is constructed, and different points on the histogram, namely the tissue peak and valley are determined. The authors note that the tissue intensity distribution, as that

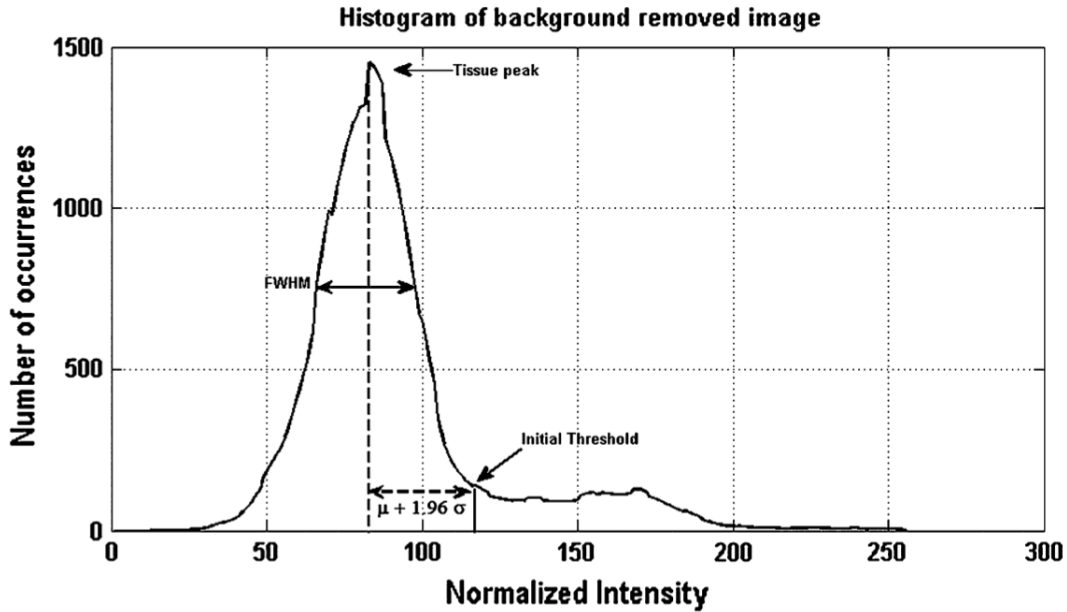


Figure 2.8: Histogram showing the tissue peak, FWHM, and initial threshold for haemorrhage slice identification and haemorrhage region segmentation [7]

seen in Figure (2.8), approximates a normal distribution. The tissue peak intensity μ is used to calculate the value of the full-width half-maximum (FWHM). The standard deviation follows the relation:

$$FWHM = 2\sigma\sqrt{2\ln 2} \quad (2.7)$$

Since 95% of the tissue region is within 1.96σ , the selected initial threshold value is $\mu + 1.96\sigma$ for the haemorrhage region. This can also be seen in the histogram shown in Figure (2.8).

Modified FCM is yet another method which can be used to segment brain haemorrhage [7]. FCM is applied on the pre-processed images where a membership matrix is generated. This membership matrix shows the extent of association samples have with each cluster. Cluster classification is done at two levels:

- The first level contains 4 clusters (C1 - C4). Cluster C1 represents CSF, cluster C2 represents GM and WM, cluster 3 represents partial volume pixels of haemorrhage and brain parenchyma pixels whilst C4 represents the haemorrhage pixels.
- In the second level, cluster C3 is subdivided into two more categories. $C3_H$ is made up of pixels that belong to the haemorrhage, whilst $C3_P$ is made up of the pixels which belong to the brain parenchyma.

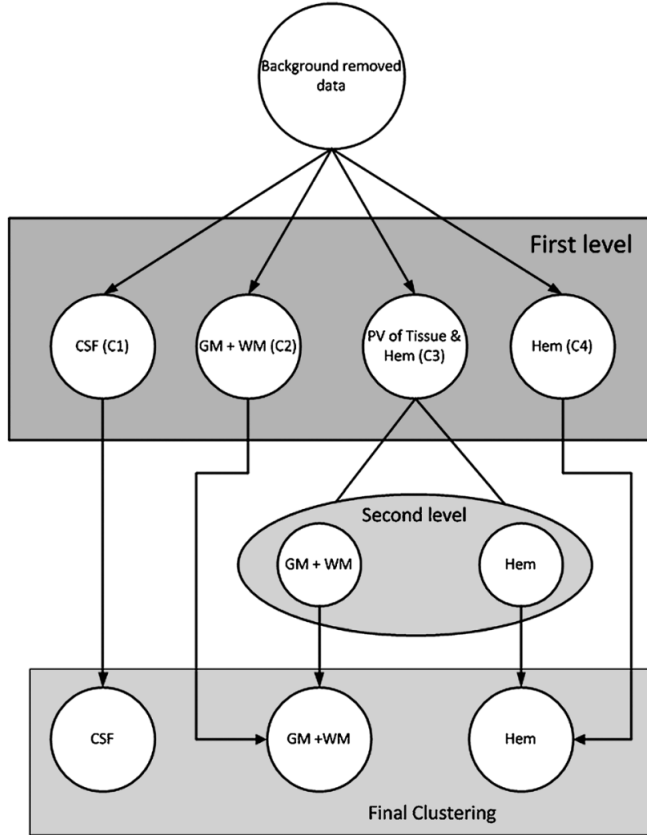


Figure 2.9: The Process of FCM Based Segmentation [7]

The classification is represented in diagram shown in Figure (2.9).

The **Modified NCut method** was proposed by Shi and Malik [39] with the aim of solving the perceptual growing problem. This method focuses on extracting the global notion of an image rather than the local one. The image segmentation is viewed as a graph partitioning problem, with NCut being the method used to segment the graph. Differences between the different groups as well as the total similarity within the groups is measured by the NCut criterion, followed by the optimisation of this criterion using a computational technique based on a generalised eigenvalue problem. NCut-based segmentation involves 3 main steps. The first step is to subject the preprocessed image to the NCut algorithm. The next step involves the obtaining of the descriptive statistics, which include the mean, standard deviation, and median of the intensities of the different regions obtained by the NCut segmentation. In the third and final step, the descriptive statistics are clustered using the FCM algorithm which allows for the merging of the different regions based on their similarities. When using NCut-based segmentation, one must specify the total amount of segments for a given slice. Prakash *et al* [7] chose 30 segments for the NCut algorithm for the initial segmentation so as

to avoid overlooking small haemorrhages. The pixels are then grouped into three clusters, these being CSF, WM and GM, and the last cluster consisting of hemorrhagic regions. The probability density function of each cluster is calculated, and the point of crossover between CSF and grey/white matter was set as the lower threshold (TH_L), whereas the cross point between white/grey matter and hemorrhagic clusters was set as the upper threshold (TH_U). Segmented regions having an intensity greater than TH_L were considered for further processing to ensure that all hemorrhagic regions are identified for post-processing. According to Prakash *et al* [7], the threshold-based method is better overall as its implementation is relatively simple and it returned the most accurate results.

The **Active Contour-based Method** is discussed by Bhaduria *et al* [37]. Active contours can be described as dynamic curves which move towards a targeted object's boundaries. The motion of the curves is controlled by internal and external forces so as to achieve a minimum energy state. This state is achieved when the curve reaches the desired object's boundaries. There are two main classes of active contour methods, these are edge-based active contour methods and region based active contour methods. Normally edge-based active contour methods consist of two parts: regularity part, and edge detection part. The shape of the contour is determined by the regularity part, whilst the edge detection part is what drives and attracts the contour towards the edges. There are various different proposed active contour methods in literature such as that proposed by Osher and Sethian [40] where curve motion is controlled by mean curvature flow, and that proposed by Caselles *et al* [41] which is an edge-based active contour method based on mean curvature motion. Bhaduria *et al* [37] compare between the thresholding method, the region growing method, FCM and the active contour-based method. They find that the thresholding method is suitable and easy to implement. However, bad tissue contrast and weak boundaries leads to false interpretation. They state that region growing gives good results but problems exist such as the selection of initial seeds and the selection of appropriate criteria to grow the regions in the image. According to the authors, FCM gives better results but the selection of the number of clusters is one of the flaws of this method. Through testing they found that the performance of the active contour based method very much depended upon the suitable contour initialisation and its propagation controlling parameters. Having said this, it was found to perform better in terms of accuracy than the other approaches investigated in this study.

3 Design & Implementation

This chapter addresses and explains different components of the implemented CAD system. The pre-processing techniques applied prior to segmentation, including noise removal and skull stripping, are explained in detail. The segmentation and detection algorithms used to detect the hemorrhagic regions are also presented together with the output that the system provides.

3.1 Overview of the Implemented CAD System

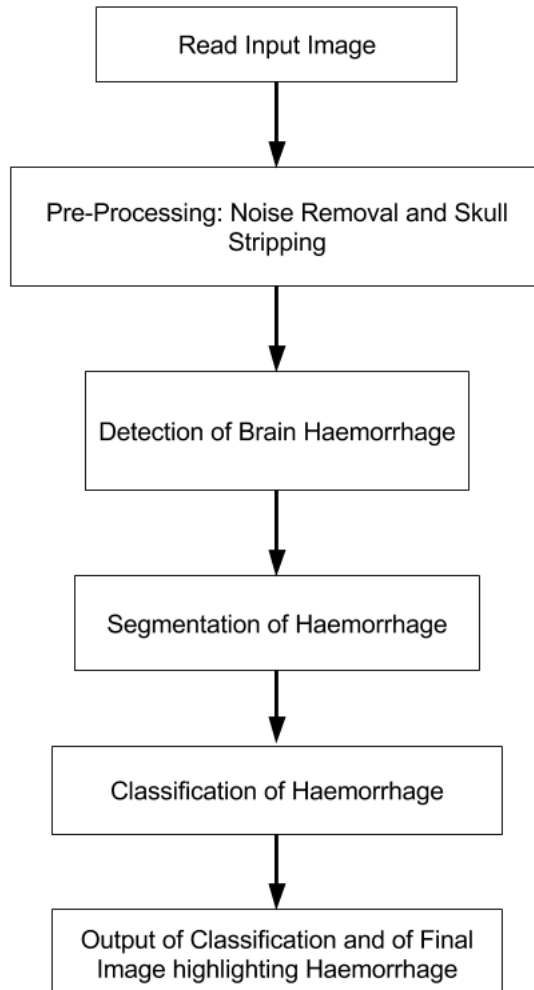


Figure 3.1: Flow Diagram of the CAD System implemented in this study

As explained in chapter two, the main steps of a CAD system involve pre-processing, detection, segmentation and output of the results. Figure (3.1) shows a flow chart of the im-

plemented CAD system using C++ in conjunction with OpenCV libraries. It is to be noted that the contrast enhancement stage has been omitted from the flow chart. The reason for this omission is that the test samples obtained already had satisfactory contrast levels. The flow chart steps and their respective implementation will be discussed in further detail later on in this chapter.

3.2 Noise Removal

In existing literature where denoising techniques are tackled, comparative measures such as peak signal-to-noise ratio (PSNR), mean square error (MSE) and the Universal Image Quality Index are used in order to compare between different techniques. In this particular study, since the original noiseless image cannot be obtained, these measuring metrics do not necessarily provide an accurate evaluation of the best performing technique.

Since one of the objectives of this project was to implement a noise removal technique as part of the pre-processing stage, a form of comparison had to be conducted between the different chosen techniques. The chosen option was that of obtaining the opinion of a qualified radiologist who would be able to indicate the technique which provided the best output. Having said this, no filter options were discarded before the final testing was completed. This was due to the fact that although visually a particular filter may seem to perform better than the others, computationally it might not provide the best results when being tested together with the segmentation and detection algorithms. The implemented techniques included the Gaussian Filter, the Median Filter, the Bilateral Filter and the Wiener Filter. These filters were chosen over other techniques based on the results from previous research in the area as well as due to the performance attributes of these filters. Other filters such as the Mean Filter and the Anisotropic Diffusion Filter were not considered due to the fact that in tests conducted by Malik *et al* [25] and Chhabra *et al* [22] their performance was inferior to that of the implemented techniques.

3.2.1 Gaussian Filtering

An implementation of the Gaussian Filter is provided by OpenCV [42]. The required parameters are the input image, an output destination image, the Gaussian kernel size and the standard deviations for the X and Y directions. The function works by convolving the input image with the Gaussian kernel. Figure (3.2b) shows an image after it was filtered using the Gaussian filter.

3.2.2 Median Filtering

OpenCV provides an implementation of the Median Filter [42]. The parameters which need to be provided are the input image, the output image destination and the aperture linear size which must be an odd number greater than 1. The image is smoothed using the median filter with the $ksize \times ksize$ aperture. Figure (3.2c) shows an image after it was filtered using the Median filter.

3.2.3 Bilateral Filtering

The bilateral filter is also provided by OpenCV [42]. The parameters required include the input image, the output image destination, the pixel neighbourhood diameter and the standard deviations for the colour and co-ordinate space. The larger the value for the colour standard deviation the more colours within the pixel neighbourhood will be mixed together, whilst a larger space standard deviation would mean that farther pixels will influence each other as long as their colours are close enough. Figure (3.2d) shows an image after it was filtered using the bilateral filter.

3.2.4 Wiener Filtering

The Wiener Filter was coded manually since there is no existing OpenCV implementation. Expanding $G(u, v)$ in equation (2.2), the resulting equation is obtained:

$$F(u, v) = \frac{H^*(u, v)}{|H(u, v)|^2 + \left[\frac{S_n(u, v)}{S_f(u, v)} \right]} \times Y(u, v) \quad (3.1)$$

where:

- $F(u, v)$ is the image in the Fourier Domain,
- $H(u, v)$ is the Fourier Transform of the sensor function, with $H^*(u, v)$ being the complex conjugate,
- $S_n(u, v)$ is the power spectrum of the noise,
- $S_f(u, v)$ is the power spectrum of the original image,
- $Y(u, v)$ is the Fourier Transform of the noisy image.

Equation (3.1) was modified by setting the sensor function and its corresponding conjugate to 1. Also, since the original noiseless image isn't known, the power spectra cannot be obtained. Therefore, an approximation must be used resulting in a constant with a value less

than 1. To apply the Wiener Filter, the noisy input image must be converted into the frequency domain. This is done using the Discrete Fourier Transform (DFT) function provided by OpenCV where the complex output is obtained. After performing the required multiplication, the Inverse DFT function provided by OpenCV is used so as to obtain the normalised real output. Figure (3.2e) shows an image filtered using the Wiener filter.

3.2.5 Selecting a Noise Reduction Method and its Corresponding Parameters

Making a choice between the different methods implemented as well as selecting the optimal parameters was not a trivial task. It had to be ensured that although noise was being reduced, the appearance of any anatomical structures would not be compromised or degraded. Keeping this in mind, the advice of qualified radiologists was sought in order to determine the best noise removal filter. A test image was chosen containing various brain features as well as brain haemorrhage. This image can be seen in Figure (3.2). For each filter, the test image was saved multiple times, each time with a different filter parameter value. Tables (3.1), (3.2), (3.3) and (3.4) show the range of parameter values used for each filtering technique. The radiologists were asked to go through these set of images per filter, and for each filter choose the image which they believed had the best diagnostic quality. Once this step was concluded, the chosen images from all the filters were grouped together, and the radiologists were asked to select the best image from all the filters.

The radiologists agreed that the Bilateral filter with a neighbourhood of 5 pixels, a colour standard deviation of 10 and a space standard deviation of 2.5 produced the image with the best quality from a medical point of view.

Gaussian Filter		
Parameter	Range	Step
Kernel Size	3x3 - 33x33	2
Standard Deviation X	0	0
Standard Deviation Y	0	0

Table 3.1: Gaussian filter parameter values tested

Median Filter		
Parameter	Range	Step
Aperture Linear Size	3x3 - 33x33	2

Table 3.2: Median filter parameter values tested

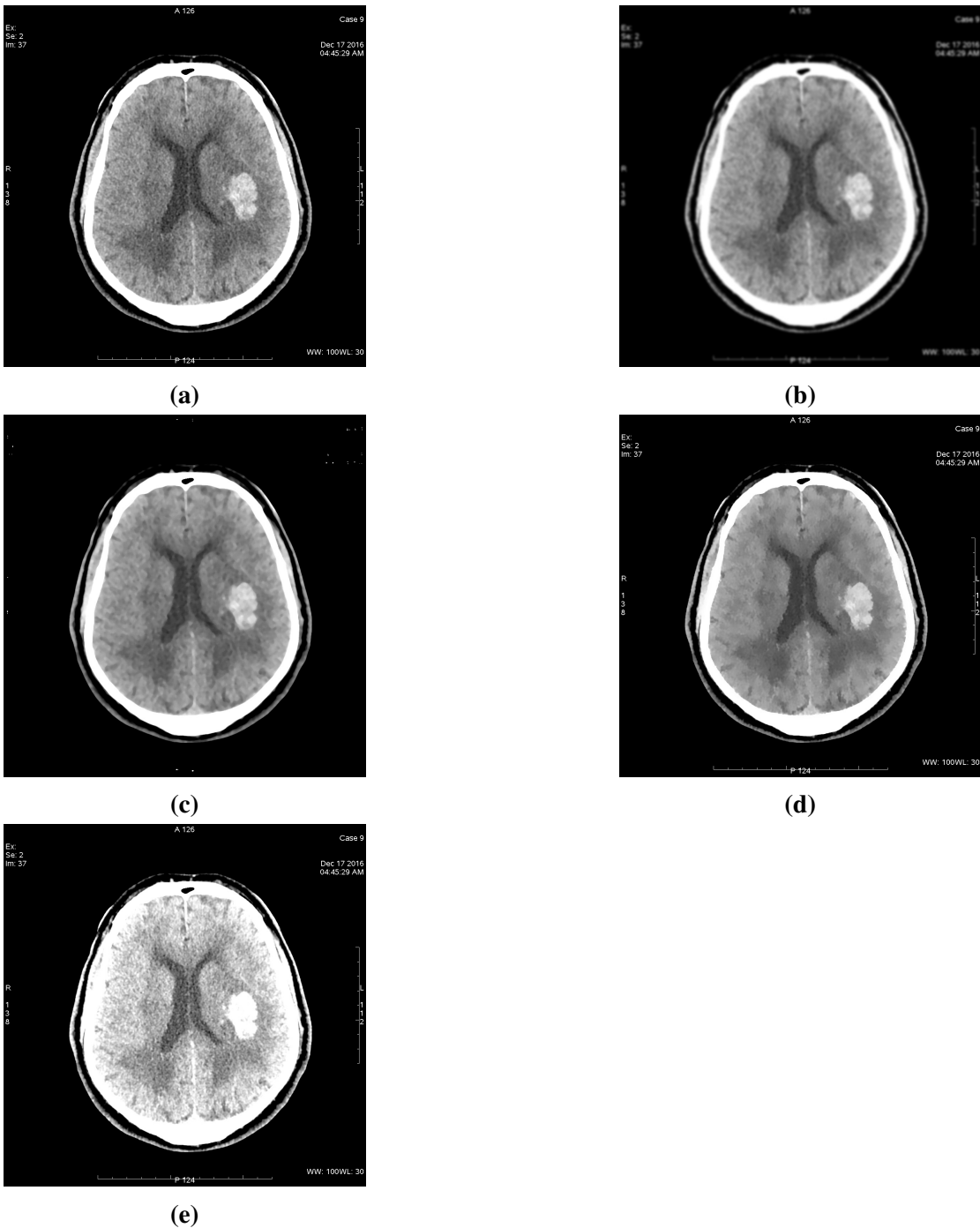


Figure 3.2: The Resulting images after filtering; (3.2a) original image, (3.2b) applying a Gaussian filer having a kernel size of 17, (3.2c) applying a Median filter having an aperture linear size of 9, (3.2d) using a Bilateral filter with a pixel neighbourhood diameter of 27, a colour standard deviation of 34 and co-ordinate space standard deviation of 13.5, (3.2e) using a Wiener filter with a constant of 0.7

Bilateral Filter		
Parameter	Range	Step
Neighbourhood	5 - 33	2
Space Variance	10 - 66	Neighbourhood \times 2
Colour Variance	2.5 - 16.5	$\frac{\text{Neighbourhood}}{2}$

Table 3.3: Bilateral filter parameter values tested

Wiener Filter		
Parameter	Range	Step
Multiplication Factor	0.5 - 0.95	0.05

Table 3.4: Wiener filter parameter values tested

3.3 Segmentation

The next step after noise removal is the segmentation stage. As discussed in chapter 2, this phase involves skull stripping and haemorrhage detection followed by segmentation. From literature analysis it is evident that there are many methods available to perform segmentation. Watershed segmentation is simple to implement. However, this method suffers from over segmentation [4] and this was clearly seen during the testing of this segmentation method. Another easily implementable method is that explained by Shahangian *et al* [5]. This method is very practical, however, it was not adopted in view that not all the test images obtained were created using the same parameters. This meant that the average pixel intensities in the images were different for every image set making extracting data from the intensity histograms very difficult. The chosen method of segmentation is similar to that proposed by Hu *et al* [3] where thresholding and contours are used in order to segment the brain from the head and skull. Erosion and dilation techniques were also incorporated in order to achieve better results. This method was selected as it was both practical to implement as well as effective in achieving segmentation of both the brain and hemorrhagic regions.

3.3.1 Removing Head Tissue and Joining Bone Structures

The first step in segmenting the brain is removing the head tissue from the skull. This was necessary as in some cases, head tissue completely surrounds the skull and its pixel values are of the same intensity as those of brain GM. This means that when a threshold was set to remove the bright intensities which make up the skull, the remaining head tissue interferes with the contour finding algorithm and in turn produces a binary mask which also included

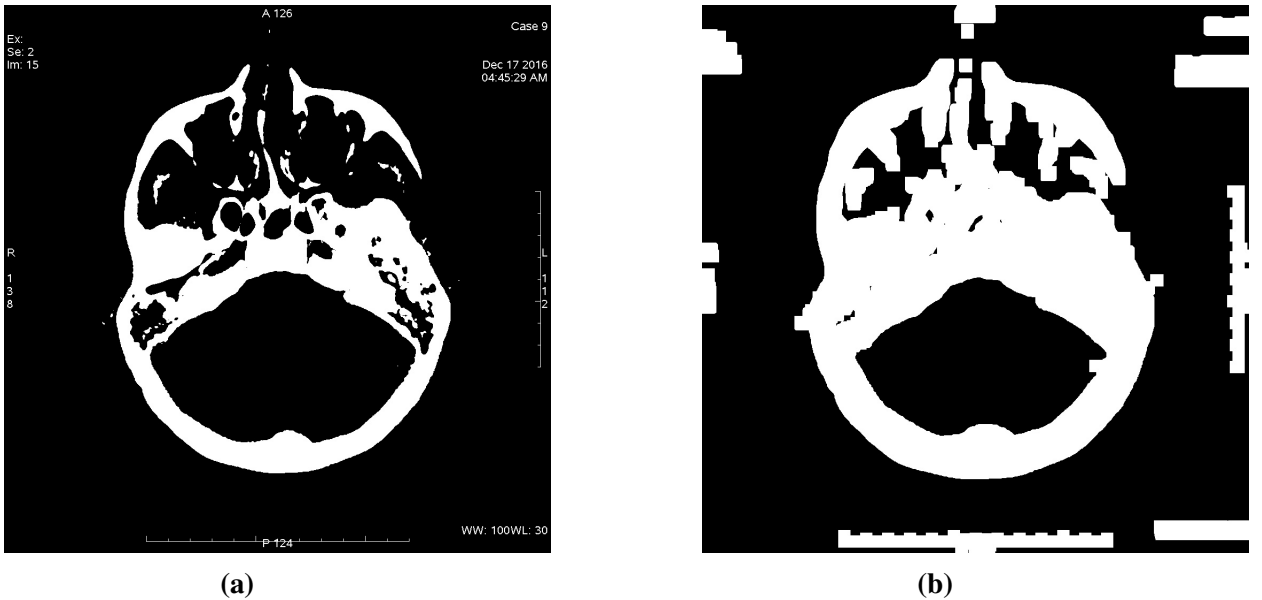


Figure 3.3: The effect of the morphological operations on the image; (3.3a) Image after applying fixed-level threshold, (3.3b) Image after applying morphological operations

the skull, hence making it redundant. Therefore to avoid this situation, the head tissue was removed by applying a fixed-level threshold on the image using the OpenCV threshold function [43]. This set to black all pixels other than the bright pixels intensities of the skull.

Once this step was completed, morphology operations were applied. The morphology operations used in the segmentation process consisted of dilation and erosion, and these were provided as functions by OpenCV [44]. Dilation is a process which involves convoluting an image α with a kernel β which has a defined anchor point. This anchor point is usually situated at the centre of the kernel [44]. The kernel β is scanned over the image, and during this process the maximum pixel value among the pixels overlapped by β is found. The image pixel in the anchor point position is replaced with this maximal value. This process therefore causes bright regions in an image to expand. This can be seen in Figure (3.3b). The erosion process is very similar but in this case the anchor point is replaced by the minimum value overlapped by β , causing bright areas in an image to shrink.

The dilation operation was required in order to join the disconnected bone structures which can be seen in Figure (3.3a). If left unmodified, the disconnected bone structure would have an adverse effect on the contour finding algorithm, with the largest contour sometimes being just the bone structure itself. Once this operation was completed, all the contours in the image were detected using the *findContours* function found in OpenCV [45]. The largest

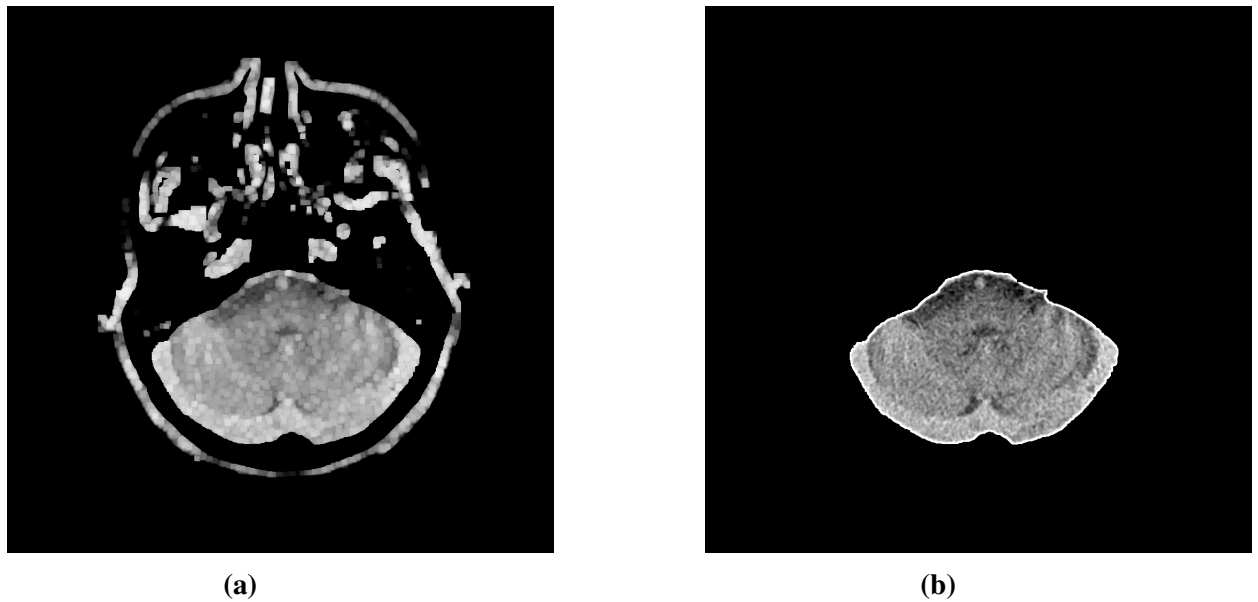
contour was determined by finding the contour with the largest pixel area using the OpenCV inbuilt *contourArea* function [46]. The segmentation procedure used the largest contour as a binary mask and applied it to the original image by setting any pixels outside the mask to black and keeping the original value of any pixels within the mask.

3.3.2 Removing the Skull

The process of removing the skull from the newly obtained image is very similar to the one described in the head tissue removal process. The first step was to set a threshold which removed the bone making up the skull whilst keeping the brain GM and WM. This was achieved by using the *Threshold to Zero, Inverted* thresholding technique. This meant that any intensities above the chosen threshold would be set to zero, meaning black in grayscale. In this case the chosen grayscale threshold value was 245, and any pixel intensities above this value were changed to 0. Erosion is then applied on the whole image in order to remove any head tissue that might still be present. The final step before segmentation can take place is once again that of dilation. This is used so as to make sure that none of the brain has been removed by the erosion process and the result of these processes can be seen in Figure (3.4a). The final segmentation process consists of finding the largest contour using the same method described in the previous subsection. The contour is set as the binary mask and as done previously, any pixels outside the mask are set to 0 and any pixels inside remain untouched. Figure (3.4b) shows the final segmented brain whilst Figures (3.5a) and (3.5b) show the original image and the segmented brain of a CT slice which contains less bone structure.

3.4 Detection

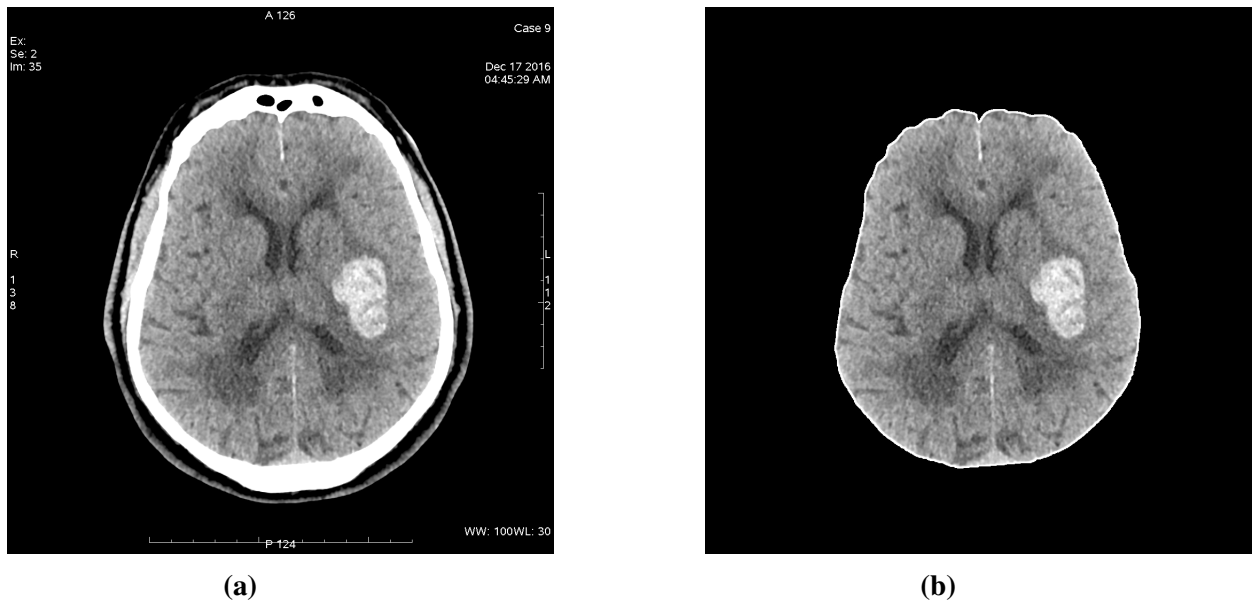
After the brain was successfully segmented from the head and skull, the haemorrhage detection phase can commence. The previous step was performed in order to increase the chances as well as the accuracy of proper detection. The aim of the study was to achieve haemorrhage detection using simple image processing techniques, and for this reason, the MDRLSE technique introduced by Prakash *et al* [34] was not considered. The Modified Threshold Method [7] was considered and tested. However, the histograms between different sets of images differed drastically. This meant that the initial threshold was not always accurate and correct results were only obtained for some of the image sets. After careful consideration, it was decided that clustering, thresholding and contour techniques would be combined to produce a functional and effective haemorrhage detection algorithm. Features such as contour area, perimeter and number of consecutive haemorrhage detections were



(a)

(b)

Figure 3.4: The removal of the skull and final brain segmentation; (3.4a) Image after removing any bones and applying erosion and dilation, (3.4b) Final segmented brain



(a)

(b)

Figure 3.5: Another example of segmenting the brain from the skull, however this time with less bone structures; (3.5a) Original unprocessed image, (3.5b) Image following segmentation processes

then used to reduce false positive results.

3.4.1 Calculating the Lower and Upper Thresholds

Detection of any haemorrhage would take place by applying a fixed-level threshold which would set all pixels which were not part of the haemorrhage to black. As mentioned earlier on, not all the obtained test image sets were created using the same parameters, which meant that pixel intensities for GM, WM and haemorrhage were different for all the CT image sets. This created a problem as a single value for the lower and upper intensity thresholds could not be used since the values would only be valid for some of the CT image sets.

The first step to solving this problem was to use a reference image with the aim of extracting initial upper and lower threshold values. The chosen image can be seen in Figure (3.5b). A clustering method was implemented in order to find the optimal lower threshold of Figure (3.5b). As done by Prakash *et al* [7] in the Modified FCM method, the pixel intensities of the image were grouped into 4 clusters. Cluster C1 represents CSF, cluster C2 represents GM and WM, cluster C3 represents partial volume pixels of haemorrhage and brain parenchyma pixels whilst C4 represents the haemorrhage pixels. The lower threshold was selected to be an intensity value found half way through the third cluster.

In the next step the average pixel intensity for Figure (3.5b) was calculated and found to be 154. This value was needed in order to check by how much the average pixel intensity differs between CT sets. An algorithm was set in place which calculated the lower threshold by first finding the pixel intensity half way through the third cluster as explained above. This was followed by setting a compensation in place for the difference in average pixel intensity. If the average pixel intensity of the image being analysed was found to be less than 154, then the lower threshold found half way through the third cluster was reduced by the same difference. Similarly, if the average pixel intensity was found to be larger than 154, the lower threshold was increased by the difference in average pixel intensities. Through testing, the upper intensity threshold was found to be 40 intensity levels greater than the lower threshold. The results of the fixed-level threshold operations can be seen in Figure (3.6).

3.4.2 Haemorrhage Detection

Before the OpenCV contour finding algorithm is used, the erosion operation is performed on the image to remove the brain outline seen in Figure (3.6b). Once this has been carried out,

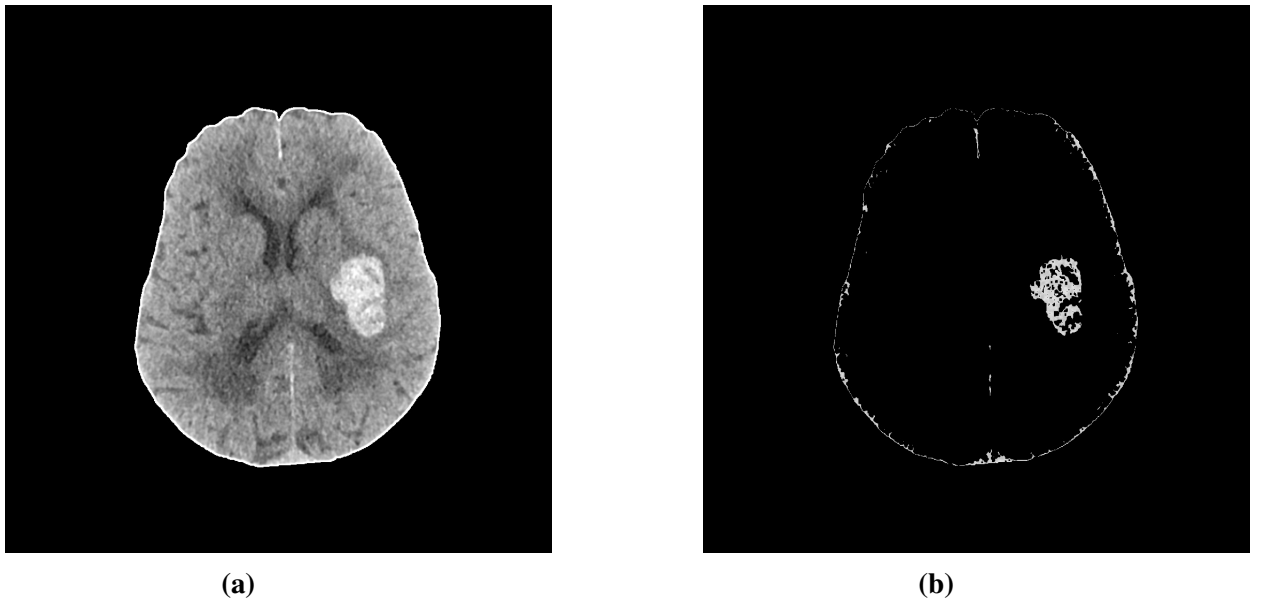


Figure 3.6: The result after applying fixed-level thresholding with the newly obtained lower and upper thresholds; (3.6a) Image following segmentation processes, (3.6b) Result obtained after applying fixed-level thresholding

the contour finding algorithm is used to obtain all the contours of joined pixel masses. From all the obtained contours the one with the largest area is selected, as whenever it is present, the hemorrhagic region forms the largest pixel mass. The contour of the entire brain is also obtained from the segmented unthresholded image. This will be used during the process of reducing false positive results.

3.4.3 Reducing False Positive Results

The above technique detects the largest pixel mass, irrelevant whether a hemorrhagic region is present or not. This means that false positive results are obtained and therefore haemorrhage characteristics need to be exploited in order to distinguish between the pathology and false results.

3.4.3.1 Contour Area

The area of the largest contour obtained was calculated using the inbuilt *contourArea* function in OpenCV. Through testing and research, it was determined that in order to be classified as a haemorrhage, the pixel mass must have an area greater than 3788 pixels. Another condition that must be satisfied is that the contour area corresponding to possible haemorrhage must be at least 10,000 pixels smaller than the contour area of the original brain. This

ensures that that brain GM and WM are not mistaken as the pathology when the skull is incorrectly segmented.

3.4.3.2 Contour Perimeter

The perimeter of the contour being considered was used to further reduce false positive results. The inbuilt *arcLength* function in OpenCV [46] was used to calculate the closed contour perimeter in terms of pixels. Two cases were considered:

The first case was used in conjunction with the above area constraints and here the perimeter of the contour being considered must be at least one and a half times smaller than the perimeter belonging to the contour of the segmented unthresholded brain. This in conjunction with the above constraints is used to differentiate between real brain haemorrhage and incorrectly detected haemorrhage. If the ROI contour area or perimeter are too similar to that of the original segmented brain, then there is a large probability that the detected largest contour consists mainly of brain WM and GM, and hence can be discarded.

The second case concerns potential haemorrhages with a contour perimeter of less than 2000 pixels. This case is only tested if the potential haemorrhage fails the joint perimeter and area case discussed above. In this instance, a contour with a closed perimeter of less than 2000 pixels must have a contour area between 2800 and 15000 pixels and the contour perimeter of the original brain must be at least 4000 pixels longer than that of the haemorrhage contour. This case is necessary as it successfully eliminates cases where no haemorrhage is present in the scan. In these cases the detected largest contour would consist of a small piece of remaining skull outline similar to that seen in Figure (3.6b).

3.4.3.3 Haemorrhage Volume

The last step in the false positive reduction process is that of eliminating false results by analysing the slice depth of a possible brain haemorrhage. Through testing carried out on the brain CT sets obtained for this study, it was noted that brain haemorrhage was present in at least four consecutive CT slices. A simple counter was implemented which would increment after every detection, and be reset to zero if no detection is made. The maximum value of the counter is saved and if haemorrhage was not detected (maximum value is less than four) in at least four consecutive slices of the CT set being analysed, all detections are discarded, and the CT set be declared free from the pathology. On the other hand, if the

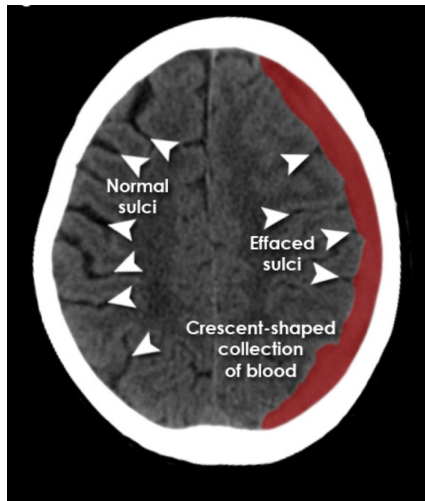


Figure 3.7: An example of extra-axial haemorrhage [8]

maximum value is four or greater, the process of highlighting the detected haemorrhage can be performed.

3.5 Classification

Brain haemorrhage can be classified into two basic groups, these being Intra-axial haemorrhage and Extra-axial haemorrhage [8]. Both groups can be broken down into further categories, each defined by the haemorrhage shape and location. The aim of the study was to implement a basic classification system which would indicate whether the detected haemorrhage was of the intra-axial type or the extra-axial type. Any further in-depth classification would require artificial intelligence techniques which were beyond the scope of this study. Intra-axial bleeding occurs inside the brain and can be seen to form abnormal shapes usually confined to a circular area, whereas extra-axial bleeding (with exception of subarachnoid haemorrhage) occurs inside the skull but outside of the brain tissue. For this reason, since it lines the skull, extra-axial haemorrhage forms a curved shape similar to that seen in Figure (3.7). This characteristic was exploited by using the solidity of the haemorrhage shape to differentiate between the two brain haemorrhage types. Since subarachnoid haemorrhage differed greatly in shape and location from the rest of the haemorrhages in the extra-axial group, it could not be correctly classified using this method and therefore was not considered in this study.

Solidity describes the extent to which a shape is convex or concave and is defined by the

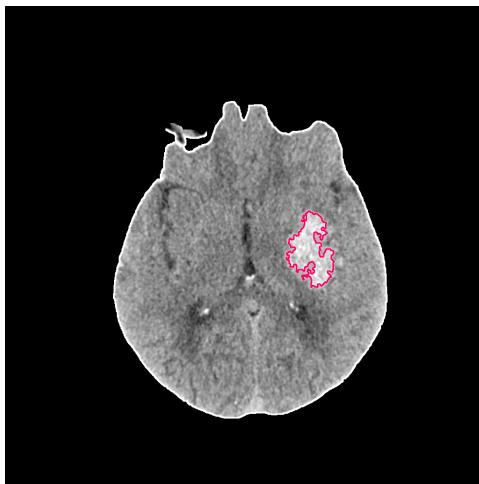
following equation:

$$Solidity = \frac{Contour\ Area}{Convex\ Hull\ Area} \quad (3.2)$$

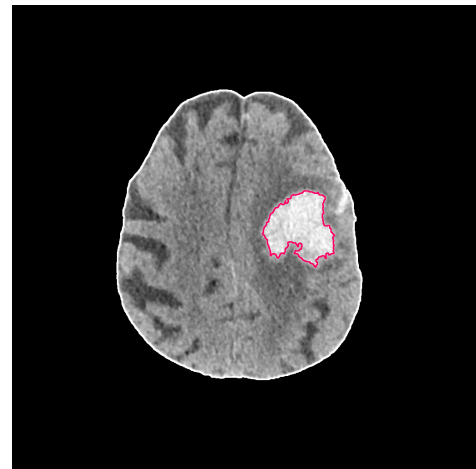
Solidity can be used to discriminate or classify regions using shape criteria since convex shapes have a solidity closer to 1 and concave shapes have a solidity closer to 0. This means that the solidity of intra-axial bleeds can be expected to be much larger than the solidity value for extra-axial bleeds. The contour area was already at hand from the previous processing steps, whilst the convex hull area needed to be calculated. The convex hull of the contour was obtained by making use of the *convexHull* OpenCV function [47] and its area was calculated by again using the *contourArea* OpenCV function. For each set where haemorrhage is present, the solidity of the haemorrhage shape is calculated per slice, and the average solidity value is obtained. Through testing, it was determined that haemorrhages which had a solidity value of less than 0.2 could be classified as extra-axial haemorrhage, whereas those with a solidity of 0.2 or greater can be classified as intra-axial haemorrhage.

3.6 Output

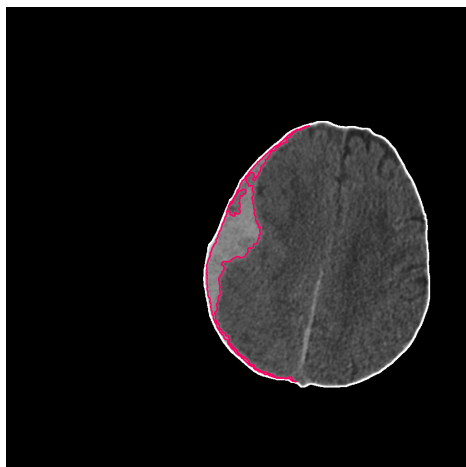
After all false positive results have been excluded, the contour lining the hemorrhagic region can be displayed and coloured in order to clearly mark the ROI. The image of the segmented brain (similar to that in Figure (3.6a)) was first converted from grayscale to a 3 channel RGB image so that colours applied to the image can be seen. The contour was then superimposed on the image through the use of the *drawContour* function in OpenCV [45]. This function draws the outline of the contour and hence indicates the boundaries of the hemorrhagic region. The contour colour chosen was a dark pink (RGB: 100,0,254) as it provided a stark contrast from the rest of the image. After the contour was successfully drawn, the image was saved in .PNG format. An example of the output can be seen in Figure (3.8). The classification of the brain haemorrhage type was provided through a command line output.



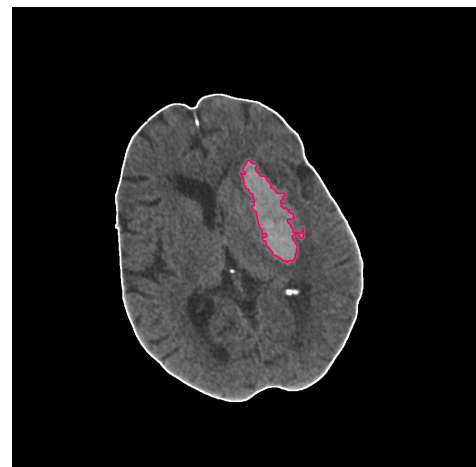
(a)



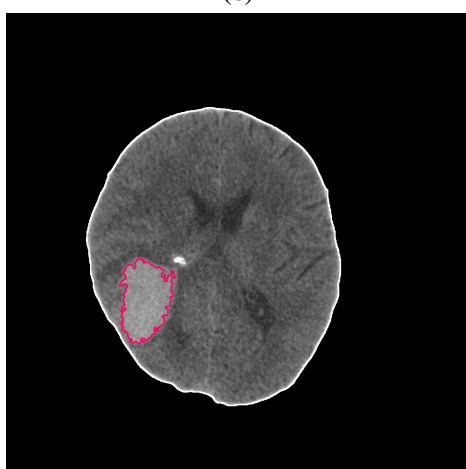
(b)



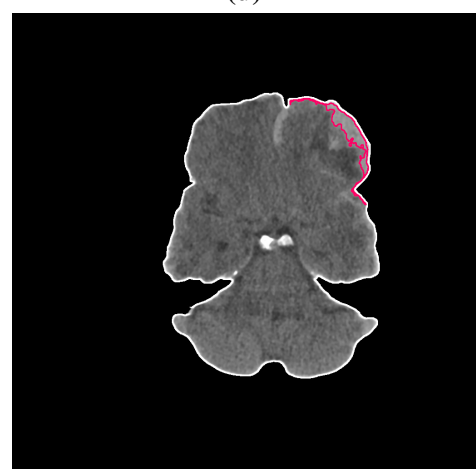
(c)



(d)



(e)



(f)

Figure 3.8: Examples of the results obtained after successfully detecting haemorrhage

4 Testing and Evaluation

Permission was granted from the general hospital in Malta to obtain and use anonymised brain CT scans. These were used to develop and test the CAD system implemented in this study. Thirty six sets from these scans were found to be suitable for this study - eighteen were normal healthy head CT sets and eighteen were CT sets containing pathology. The latter contained different types of haemorrhage so that the CAD system could be tested for robustness when encountering different haemorrhage types.

4.1 Results

The measures used to evaluate the results obtained in this study were **sensitivity**, **specificity** and **precision**. These measures are defined and calculated through the following equations:

$$Sensitivity = \frac{True\ Positive}{True\ Positive + False\ Negative} \quad (4.1)$$

$$Specificity = \frac{True\ Negative}{True\ Negative + False\ Positive} \quad (4.2)$$

$$Precision = \frac{True\ Positive}{True\ Positive + False\ Positive} \quad (4.3)$$

When dealing with the brain haemorrhage detection aspect of the CAD system, *True Positive* refers to a correctly detected haemorrhage. *False Positive* indicates that haemorrhage was detected by the system in a case where no haemorrhage was in fact present. In the case of a *False Negative* result, any present haemorrhage would not have been detected by the CAD system. A result is deemed *True Negative* if the system correctly indicates that no haemorrhage is in fact present.

In the case of the classification part of the system, a detected haemorrhage would always be deemed either an intra-axial or an extra-axial haemorrhage. This meant that the possible results were that of a correct classification or an incorrect one. Hence, the results were computed as a simple percentage of correct classifications.

The sensitivity and precision were calculated using those CT sets containing haemorrhage. From the 18 sets containing the pathology, haemorrhage was successfully detected in all but one of the sets. The sensitivity of the system was calculated to be 94.4% whilst the preci-

sion obtained was that of 91.259%. The classification accuracy for the same sets was also calculated and found to be 88.89%. The specificity of the system was calculated using those CT sets which contained healthy normal brains and was calculated to be 94.4%.

A typical output obtained from the CAD system can be seen in Figure (4.1). This particular CT set shows a clear case of intra-axial haemorrhage. As in most cases, there is a single bleed which increases and decreases in area as the CT slices progress. When analysing the system output, it can be noticed that the CAD system correctly detects the haemorrhage and therefore this is considered as a true positive result. Figure (4.2) shows the last 4 image slices of the same CT set where a false positive result was recorded.

The true positive results can be seen in Figures (4.1b) through (4.1g). In this case the haemorrhage was correctly detected and the hemorrhagic region outlined. In Figures (4.1a) and (4.1h)) the pink arrows indicate the location of the haemorrhage and show where it begins to form and where it fades away. In these two cases the haemorrhage is too small and therefore does not meet the requirements of the CAD system. In Figure (4.2) the last four images of the CT set discussed in Figure (4.1) can be seen. A false positive result is indicated by the green arrow in Figure (4.2d) as the system has incorrectly detected haemorrhage. In this image no bleeding is present, and the incorrect detection has occurred as a result of the bone structure still being present after the brain segmentation phase. The classification output obtained was intra-axial haemorrhage meaning that the correct result was obtained.

The performance of the CAD system regarding execution time was also evaluated. All the obtained CT images were 1024 pixels wide and 1024 pixels long (1024×1024) whereas the number of images per CT set differed. This meant that the time taken by the system to run was mostly affected by the amount of images per set. The time taken for the system to complete each test from file input to file output was recorded.

The CT set with the least amount of slices contained 20 images and this set took about 5.21 seconds to run. The largest CT set contained a total of 57 images and took approximately 11.75 seconds to run, this being the longest time to complete the entire operation. All tests were performed using an Intel Core i7-4770HQ CPU clocked at 2.2GHz.

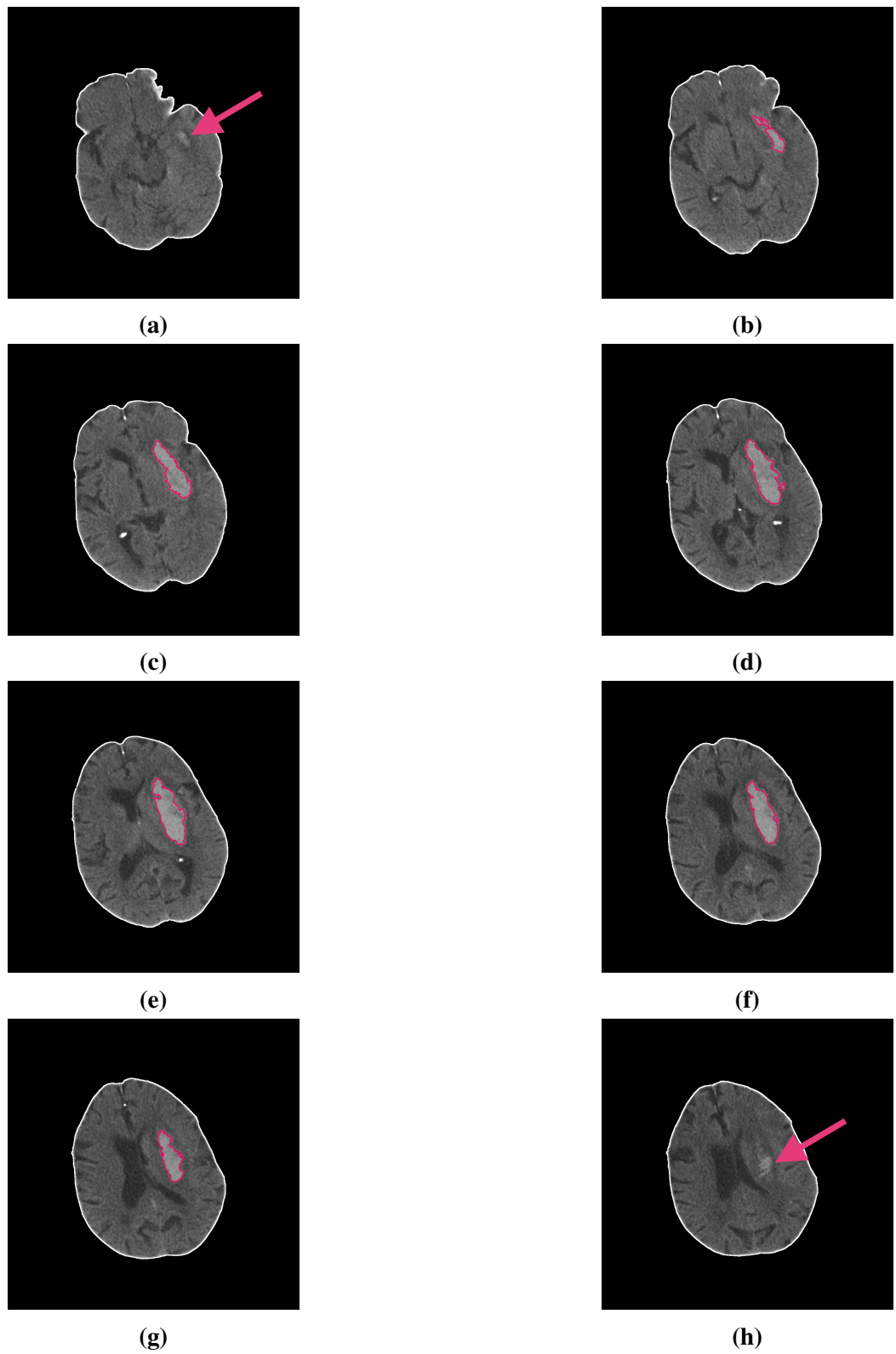


Figure 4.1: Typical output obtained from the CAD system

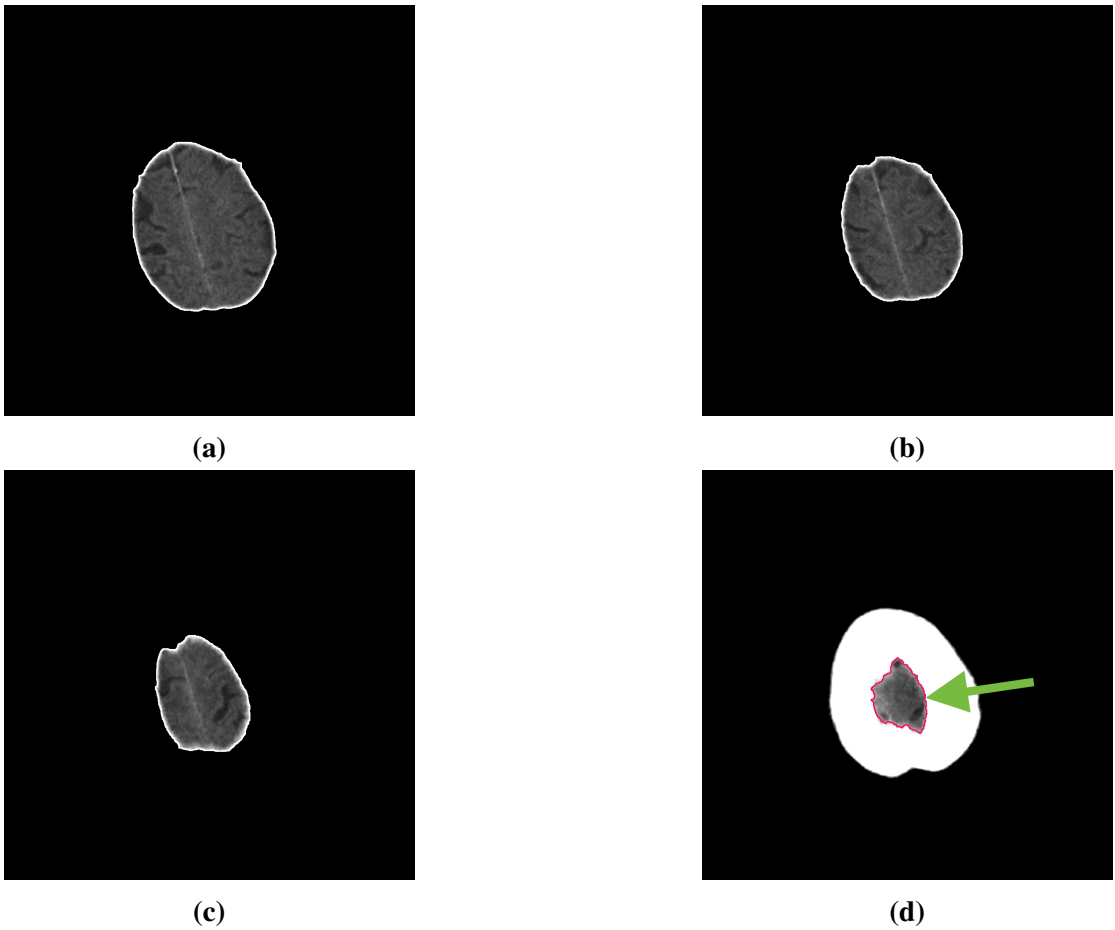


Figure 4.2: Last four image slices of the CT set seen in Figure (4.1)

4.2 Comparison with other CAD Systems

Literature does exist regarding performance of brain haemorrhage detection techniques and of CAD systems. Bhaduria *et al* [37] provided results in terms of average sensitivity and specificity of various segmentation methods used for haemorrhage detection. The segmentation methods tested are Thresholding, Region Growing, Fuzzy Clustering and the Level Set Method. A similar comparison was conducted by Prakash *et al* [7] where the effectiveness of the Modified Threshold Method, Modified FCM and Modified NCut are tested in order to obtain their sensitivity and specificity in connection with automatic haemorrhage segmentation. Shahangian *et al* [5] created and provide the results of a CAD system for the automatic detection and classification of EDH, ICH and SDH brain haemorrhages. Table (4.1) lists the mentioned results as well as the results obtained in this study.

Regarding sensitivity, the obtained results surpass all the compared literature. This may be possibly due to the other studies taking into consideration whether haemorrhage was de-

Results		
Study	Sensitivity	Specificity
Bhadauria <i>et al</i> [37] (Thresholding)	71.24%	98.22%
Bhadauria <i>et al</i> [37] (Region Growing)	73.55%	97.98%
Bhadauria <i>et al</i> [37] (Fuzzy Clustering)	76.21%	98.66%
Bhadauria <i>et al</i> [37] (Level Set Method)	77.57%	98.92%
Prakash <i>et al</i> [7] (Modified Threshold)	84.06%	99.93%
Prakash <i>et al</i> [7] (Modified FCM)	80.84%	99.83%
Prakash <i>et al</i> [7] (Modified NCut)	83.80%	99.79%
Shahangian <i>et al</i> [5]	85.267%	96.053 %
This Study	94.4%	94.4 %

Table 4.1: Comparison between the results obtained in this study, and those from other studies

tected and present in each and every CT slice. This study focused on obtaining a correct diagnosis since the purpose of the implemented CAD system was that of a supportive tool. Therefore, if the system was able to correctly detect haemorrhage anywhere in the CT set then the result was considered to be enough to bring the detected area to the attention of the radiologist, and hence considered to be a success.

The obtained result for specificity was slightly below those obtained by the mentioned studies. However, since the difference is very small, the result was considered to be satisfactory.

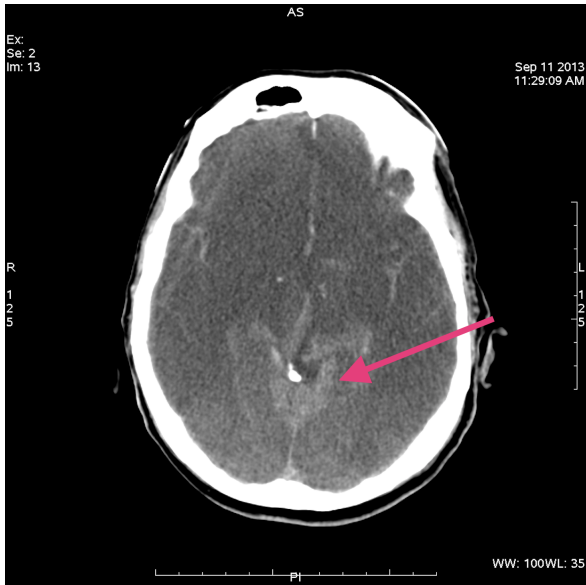
4.3 Observations

4.3.1 CT Image Contrast

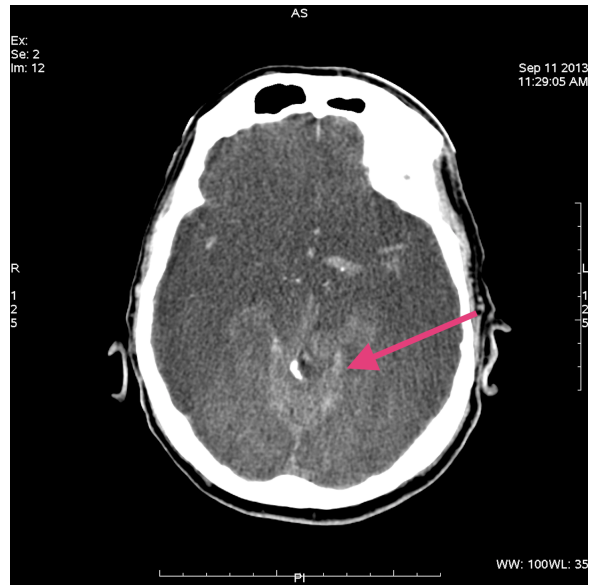
Through testing it was noted that the image contrast can have a big effect on the performance of the developed system. The reason that brain CT image sets can have different contrasts is because in some cases contrast medium in the form of a liquid is injected intravenously to allow for better delineation of structures. The images in Figure (4.3) show an example of a false negative result. The poor contrast in this particular CT set meant that the CAD system was not able to detect any haemorrhage (as that pointed at by the pink arrows) in any of the CT slices. This problem occurred since the developed algorithm for haemorrhage detection was dependent on the intensity pixel values of the hemorrhagic area as well as the difference in intensity values between this area and the brain GM and WM.

4.3.2 Skull Outline Effect on False Positives

In some cases the skull outline which remains after the brain segmentation phase can effect the algorithm which determines whether haemorrhage is present or not. A clear example

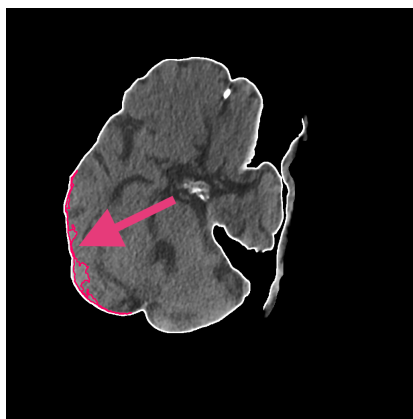


(a)

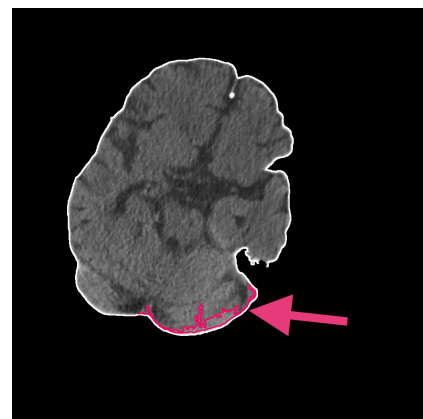


(b)

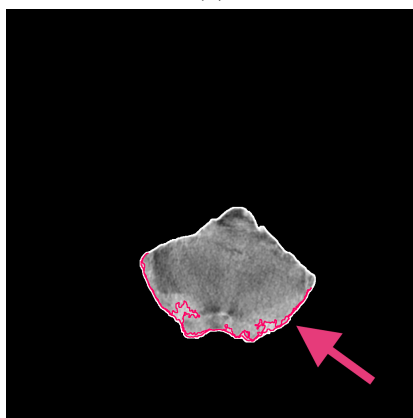
Figure 4.3: An example of low contrast CT images of a brain which contains haemorrhage



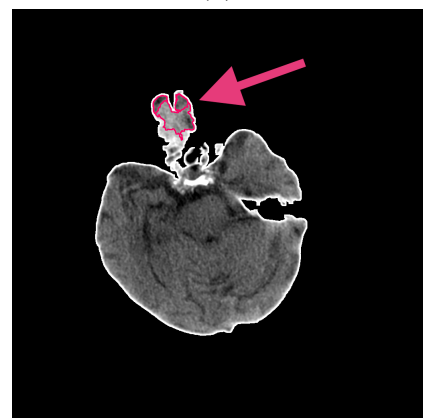
(a)



(b)

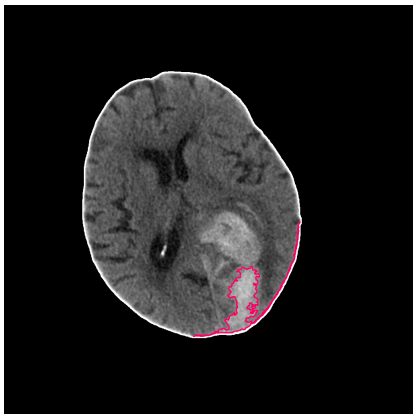


(c)

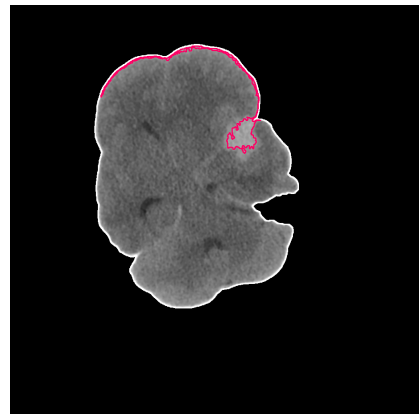


(d)

Figure 4.4: An example of a false positive result which occurred due to the skull outline



(a)



(b)

Figure 4.5: An example of how the skull pixels can effect the shape of the contour

can be seen in the images found in Figure (4.4). The incorrect results occur when there is an area of brain GM and WM pixels located close to the skull which have a slightly brighter intensity. The brighter intensity of these pixels is an anomaly which can also be caused by an artefact such as a beam-hardening and scatter artefact or a movement artefact.

4.3.3 Skull Outline Effect on Classification

Classification results can be slightly effected by the skull outline. The elongated contour outline seen in Figures (4.5a) and (4.5b) is due to the haemorrhage pixels being very close to the skull pixels. The algorithm therefore mistakes some of the bright skull pixels for haemorrhage pixels and includes them inside the contour. The elongated contour reduces the solidity of the contour, and in extreme cases can have an effect large enough to misclassify an intra-axial haemorrhage for an extra-axial haemorrhage.

5 Conclusion and Future Work

This chapter gives an overview of the developed CAD system including the results obtained. Different approaches than those implemented will be discussed including suggestions on areas for possible future improvement.

5.1 CAD System Overview and Conclusion

As mentioned in the first chapter of this study, brain haemorrhage is a serious and potentially deadly health issue affecting many people each year. This means that the findings of this study and that of any other work in the same area can be positively implemented with the aim of saving lives. Having said this, the purpose of this extensive study was to detail the development of a CAD system that detects and provides basic classification of brain haemorrhage in brain CT scans, through the use of basic image processing techniques. Hence the main aim of this study was the successful implementation of the system. The main procedures performed by the implemented CAD system can be summarised in the following:

- The .PNG image is loaded and read.
- The image quality is improved by removing noise through the use of a Bilateral Filter.
- The brain is segmented from the head and skull through the use of fixed-level thresholding, contour techniques, erosion and dilation.
- Possible haemorrhage is segmented using a combination of clustering, thresholding and contour techniques.
- Actual brain haemorrhage is detected and highlighted using false positive reduction by taking into consideration the contour area, contour perimeter and haemorrhage volume.
- Basic haemorrhage classification takes place through the use of haemorrhage solidity.
- The system outputs the segmented brain images with the haemorrhage outlined (if present), and any classification is outputted through command line output.

During this study 36 brain CT sets were used for the purpose of testing. The results achieved included a sensitivity of 94.4%, a specificity of 94.4%, a precision of 91.259% and a classification accuracy of 88.89%. It was noted that the time taken by the system to complete

a run was dependent on the number of slices in a CT set. Testing showed that for a CT set containing 20 images, the full results were obtained after 5.21 seconds whereas for a set containing 57 images, the full results were obtained after 11.75 seconds. Through analysis of these results, ways in which the system could be improved were explored. The outcome of this analysis is explained in the next section.

The developed system was compared to haemorrhage segmentation techniques reported by Bhaduria *et al* [37] and Prakash *et al* [7] and to the CAD system developed by Shahangian *et al* [5]. The sensitivity obtained by the system developed in this study was superior to all the compared techniques and systems presented by these studies. On the other hand, the specificity was found to be slightly lower but still comparable to the results obtained by the compared studies.

5.2 Future Work

Changes and enhancements may be implemented on the developed CAD system in order to possibly improve on the results obtained with the current solution. Further research is necessary as there is no certainty that these potential areas of improvements will obtain improved results.

5.2.1 Exploiting the Characteristics of the Bleed

Haemorrhage is usually present in several consecutive CT slices and this is the reason why in its current form, the implemented CAD system takes into consideration the amount of consecutive haemorrhage detections in different CT slices. However, another feature of a hemorrhagic bleed can be noted and therefore exploited. This feature is the manner in which the amount of blood fluctuates as the CT slices progress. Analysing the initial slices where haemorrhage has been detected, it can be noted that the amount of blood and hence the area taken up by the blood, is small. In subsequent slices, the amount of blood present in each slice can be seen to gradually increase before reaching a maximum. After this, the area occupied by the blood in the remaining slices usually decreases as the slices progress, before eventually disappearing. Therefore, if the areas occupied by the bleed in each slice were to be plotted against the slice number, one would end up with a plot containing a curve close to a normal distribution. This means that the area of each haemorrhage detection per slice can be calculated, and the shape of the resulting curve be compared to the shape of the normal distribution. If implemented, this would be a robust false positive reduction technique due to the inconsistent area values per slice of false positive results.

5.2.2 Contrast Check

An issue encountered during the system implementation and testing was that not all of the CT sets were created using the same parameters. Regarding contrast, this meant that the contrast enhancement varied greatly from set to set. Some of the CT sets had acceptable contrast values, whereas in others the contrast was not enhanced enough. The current system can be improved by including a contrast check in the preprocessing stage, prior to brain segmentation. This check would analyse the contrast values and if they are found to be acceptable, the rest of the system procedures would continue normally. On the other hand, if the contrast is not within an acceptable range, then contrast enhancement is applied to bring the values within the desired range. This would lead to much better results in the detection process and reduce the occurrence of false positive results.

5.2.3 Artificial Intelligence techniques for classification

The current classification algorithm only takes into consideration the shape of the haemorrhage. In view of this, Subarachnoid haemorrhage cannot be correctly classified as an extra-axial haemorrhage due to it differing greatly in shape from the other haemorrhages in that group. Another drawback of the current classification system is that it can only classify haemorrhages as intra-axial or extra-axial. It cannot provide a more in depth classification. Through the implementation of Artificial Intelligence (AI) techniques, both the haemorrhage shape and location can be taken into consideration to be able to provide a more holistic and in-depth classification than just the intra-axial and extra-axial classes. The individual haemorrhages within those classes would be able to be distinguished and classified due difference in their characteristics.

5.2.4 Parallelisation of Processes

Although the execution time for developed CAD system is acceptable, parallelisation techniques can be introduced to further reduce this time. Several procedures such as the output and classification procedures can be parallelised in order to possibly achieve results in almost real time. This will not only speed up the CAD system itself, but it will also positively affect the time taken for diagnosis meaning that it will benefit both radiologists and patients alike.

5.2.5 Detecting older haemorrhages

This study focuses on detecting and classifying fresh haemorrhages which form a white hyper-dense area on the CT scan. Future work can be extended to include haemorrhages

which are no longer fresh and are seen to form a dark area on a CT scan. In such cases both the dark intensity of the pixels as well as the symmetry of the brain need to be taken into consideration.

References

- [1] “Computed Tomography Image Quality Optimization and Dose Management.” <http://www.sprawls.org/resources/CTIQDM>. [Online; Accessed: 2016-12-26].
- [2] “Acute CT Brain.” http://www.radiologymasterclass.co.uk/tutorials/ct/ct_acute_brain/ct_brain_cerebral_haemorrhage#top_2nd_img. [Online; Accessed: 2017-05-18].
- [3] Q. Hu, G. Qian, A. Aziz, and W. L. Nowinski, “Segmentation of brain from computed tomography head images,” in *Engineering in Medicine and Biology Society, 2005. IEEE-EMBS 2005. 27th Annual International Conference of the*, pp. 3375–3378, IEEE, 2006.
- [4] W. M. D. W. Zaki, M. F. A. Fauzi, R. Besar, and W. S. H. M. W. Ahmad, “Qualitative and quantitative comparisons of haemorrhage intracranial segmentation in CT brain images,” in *TENCON 2011 - 2011 IEEE Region 10 Conference*, pp. 369–373, Nov 2011.
- [5] B. Shahangian and H. Pourghassem, “Automatic brain hemorrhage segmentation and classification in CT scan images,” in *2013 8th Iranian Conference on Machine Vision and Image Processing (MVIP)*, pp. 467–471, Sept 2013.
- [6] X. Zang, Y. Wang, J. Yang, and Y. Liu, “A novel method of CT brain images segmentation,” in *2010 International Conference of Medical Image Analysis and Clinical Application*, pp. 109–112, June 2010.
- [7] B. P. KN, J. Hu, T. C. Morgan, D. Hanley, and W. L. Nowinski, “Comparison of 3-segmentation techniques for intraventricular and intracerebral hemorrhages in unenhanced computed tomography scans,” *Journal of Computer Assisted Tomography*, vol. 36, no. 1, pp. 109–120, 2012.
- [8] “Intracranial Haemorrhage.” <https://radiopaedia.org/articles/intracranial-haemorrhage>. [Online; Accessed: 2017-04-14].
- [9] P. Armstrong, M. Wastie, and A. G. Rockall, *Diagnostic imaging*. John Wiley & Sons, 2010.
- [10] Nowinski, Wieslaw L and Qian, Guoyu and Hanley, Daniel F, “A CAD System for Hemorrhagic Stroke,” *The Neuroradiology Journal*, vol. 27, no. 4, pp. 409–416, 2014.

- [11] Doi, Kunio, “Computer-aided diagnosis in medical imaging: historical review, current status and future potential,” *Computerized Medical Imaging and Graphics*, vol. 31, no. 4, pp. 198–211, 2007.
- [12] Honeyman-Buck, Janice, “Transforming the radiological interpretation process: TRIP—Where are we now?,” in *SPIE Medical Imaging*, pp. 76280R–76280R, International Society for Optics and Photonics, 2010.
- [13] Li, Feng and Aoyama, Masahito and Shiraishi, Junji and Abe, Hiroyuki and Li, Qiang and Suzuki, Kenji and Engelmann, Roger and Sone, Shusuke and MacMahon, Heber and Doi, Kunio, “Radiologists’ performance for differentiating benign from malignant lung nodules on high-resolution CT using computer-estimated likelihood of malignancy,” *American Journal of Roentgenology*, vol. 183, no. 5, pp. 1209–1215, 2004.
- [14] “Computed Tomography (CT) Scans and Cancer.” <https://www.cancer.gov/about-cancer/diagnosis-staging/ct-scans-fact-sheet>. [Online; Accessed: 2017-04-18].
- [15] Dendy, Philip Palin and Brian Heaton, *Physics for diagnostic radiology*. CRC Press, 2011.
- [16] “What are the Radiation Risks from CT?.” <https://www.fda.gov/radiation-emittingproducts/radiationemittingproductsandprocedures/medicalimaging/medicalx-rays/ucm115329.htm>. [Online; Accessed: 2017-04-20].
- [17] Stockley, Corinne and Oxладе, Chris and Wertheim, Jane and Smith, Guy and Chen, Kuo Kang and Rogers, Kirsteen, *The Usborne Illustrated Dictionary of Science*. Usborne, 2001.
- [18] “What causes hemorrhage? 36 possible conditions.” <http://www.healthline.com/symptom/hemorrhage>. [Online; Accessed: 2017-04-20].
- [19] M. Diwakar and M. Kumar, “CT image noise reduction based on adaptive wiener filtering with wavelet packet thresholding,” in *2014 International Conference on Parallel, Distributed and Grid Computing*, pp. 94–98, Dec 2014.
- [20] M. K. Kalra, M. M. Maher, and T. L. Toth, “Strategies for CT radiation dose optimization,” *Journal of Radiology*, vol. 230, no. 3, pp. 619–628, 2004.
- [21] A. Borsdorf, R. Raupach, T. Flohr, and J. Hornegger, “Wavelet based noise reduction in CT-images using correlation analysis,” *IEEE Transactions on Medical Imaging*, vol. 27, pp. 1685–1703, Dec 2008.

- [22] T. Chhabra, G. Dua, and T. Malhotra, “Comparative analysis of methods to denoise ct scan images,” *International Journal of Advanced Research in Electrical, Electronics and Instrumentation Engineering*, vol. 2, pp. 3363–3369, July 2013.
- [23] S. H. Teoh, “Exploration of current trend on median filtering methods utilized in digital grayscale image processing,” *International Journal of Machining and Machinability of Materials*, vol. 1, pp. 50–54, 2013.
- [24] D. R. K. Brownrigg, “The weighted median filter,” *Communications of the ACM*, vol. 27, pp. 804–828, August 1984.
- [25] S. H. Malik, T. A. Lone, and S. Quadri, “Contrast enhancement and smoothing of CT images for diagnosis,” in *2nd International Conference on Computing for Sustainable Global Development*, pp. 2214–2219, IEEE, 2015.
- [26] A. K. Jain, *Fundamentals of Digital Image Processing*. Prentice Hall, 1989.
- [27] X. Zhang and Y. Xiong, “Impulse noise removal using directional difference based noise detector and adaptive weighted mean filter,” *IEEE Signal Processing Letters*, vol. 16, pp. 295–298, April 2009.
- [28] S. K. Weeratunga and C. Kamath, “Comparison of PDE-based non-linear anisotropic diffusion techniques for image denoising,” *Proc. SPIE*, vol. 5014, pp. 201–212, 2003.
- [29] T.-L. Tan, K.-S. Sim, and A.-K. Chong, “Contrast enhancement of ct brain images for detection of ischemic stroke,” in *International Conference on Biomedical Engineering (ICoBE)*, pp. 385–388, February 2012.
- [30] G. Zhang, P. Yan, H. Zhao, and X. Zhang, “A contrast enhancement algorithm for low-dose ct images based on local histogram equalization,” in *2008 2nd International Conference on Bioinformatics and Biomedical Engineering*, pp. 2462–2465, May 2008.
- [31] S. Mukhopadhyay, N. Ghosh, R. Burman, P. K. Panigrahi, S. Pratiher, M. Venkatesh, S. Mandal, and S. Changdar, “An optimized hyper kurtosis based modified duo-histogram equalization (HKMDHE) method for contrast enhancement purpose of low contrast human brain CT scan images,” in *2015 International Conference on Advances in Computing, Communications and Informatics (ICACCI)*, pp. 1819–1821, IEEE, 2015.
- [32] A. Kaur, A. Girdhar, and N. Kanwal, “Region of Interest Based Contrast Enhancement Techniques for CT Images,” in *2016 Second International Conference on Computational Intelligence & Communication Technology (CICT)*, pp. 60–63, IEEE, 2016.

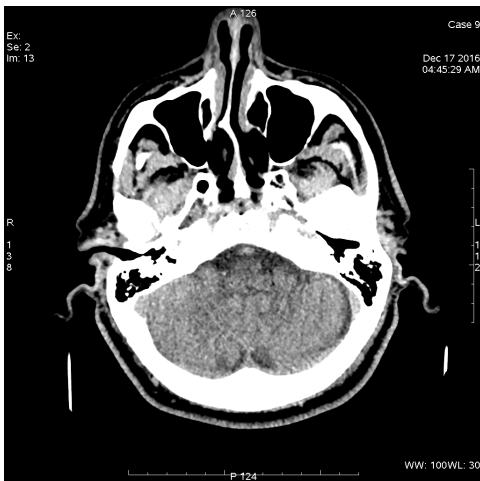
- [33] S. S. Al-amri, N. Kalyankar, and S. Khamitkar, “Linear and non-linear contrast enhancement image,” *International Journal of Computer Science and Network Security*, vol. 10, no. 2, pp. 139–143, 2010.
- [34] K. N. B. Prakash, S. Zhou, T. C. Morgan, D. F. Hanley, and W. L. Nowinski, “Segmentation and quantification of intra-ventricular/cerebral hemorrhage in CT scans by modified distance regularized level set evolution technique,” *International Journal of Computer Assisted Radiology and Surgery*, vol. 7, no. 5, pp. 785–798, 2012.
- [35] A. Lauric and S. Friskin, “Soft segmentation of CT brain data,” *Tufts University*, 2007.
- [36] N. Otsu, “A threshold selection method from gray-level histograms,” *Automatica*, vol. 11, no. 285-296, pp. 23–27, 1975.
- [37] N. S. Bhaduria, M. S. Bist, R. B. Patel, and H. S. Bhaduria, “Performance evaluation of segmentation methods for brain CT images based hemorrhage detection,” in *2015 2nd International Conference on Computing for Sustainable Global Development (INDIACoM)*, pp. 1955–1959, March 2015.
- [38] C. Li, C. Xu, C. Gui, and M. D. Fox, “Distance Regularized Level Set Evolution and Its Application to Image Segmentation,” *IEEE Transactions on Image Processing*, vol. 19, pp. 3243–3254, Dec 2010.
- [39] J. Shi and J. Malik, “Normalized cuts and image segmentation,” in *Proceedings of IEEE Computer Society Conference on Computer Vision and Pattern Recognition*, pp. 731–737, Jun 1997.
- [40] S. Osher and J. A. Sethian, “Fronts propagating with curvature-dependent speed: algorithms based on hamilton-jacobi formulations,” *Journal of computational physics*, vol. 79, no. 1, pp. 12–49, 1988.
- [41] V. Caselles, F. Catté, T. Coll, and F. Dibos, “A geometric model for active contours in image processing,” *Numerische mathematik*, vol. 66, no. 1, pp. 1–31, 1993.
- [42] “Image Filtering.” <http://docs.opencv.org/2.4.8/modules/imgproc/doc/filtering.html>. [Online; Accessed: 2017-04-15].
- [43] “Threshold.” http://docs.opencv.org/2.4/modules/imgproc/doc/miscellaneous_transformations.html?highlight=threshold#threshold. [Online; Accessed: 2017-04-15].

- [44] “Eroding and Dilating.” http://docs.opencv.org/2.4/doc/tutorials/imgproc/erosion_dilatation/erosion_dilatation.html. [Online; Accessed: 2017-04-14].
- [45] “Structural Analysis and Shape Descriptors.” http://docs.opencv.org/2.4/modules/imgproc/doc/structural_analysis_and_shape_descriptors.html?highlight=findcontours. [Online; Accessed: 2017-04-15].
- [46] “Contour Features.” http://docs.opencv.org/trunk/dd/d49/tutorial_py_contour_features.html. [Online; Accessed: 2017-04-15].
- [47] “Structural Analysis and Shape Descriptors.” http://docs.opencv.org/2.4/modules/imgproc/doc/structural_analysis_and_shape_descriptors.html?highlight=convexhull#convexhull. [Online; Accessed: 2017-04-14].

Appendix

(A) A Whole Brain CT Scan Set

The following is a brain CT set consisting of 45 slices. Each image has a dimension of 1024×1024 and is in .PNG format. Any hemorrhagic region present in any of the slices is indicated by the pink arrow.



(1)



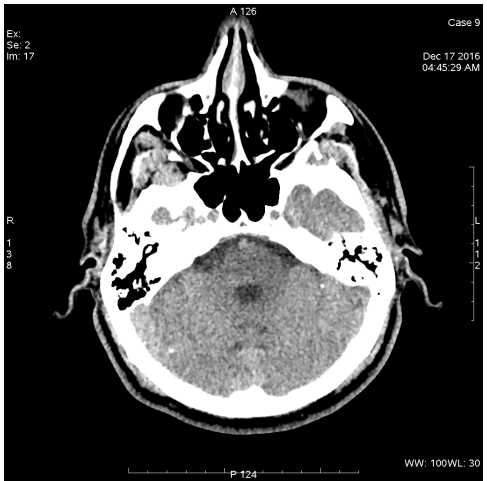
(2)



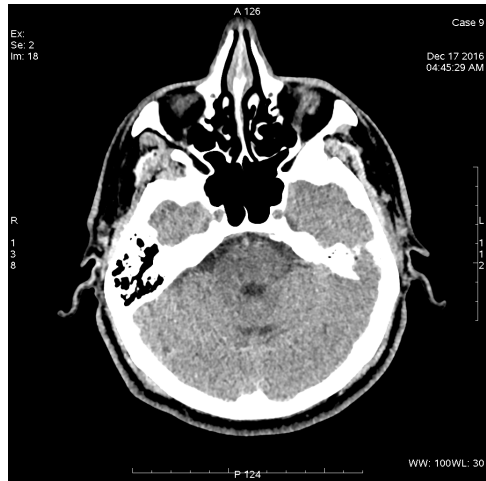
(3)



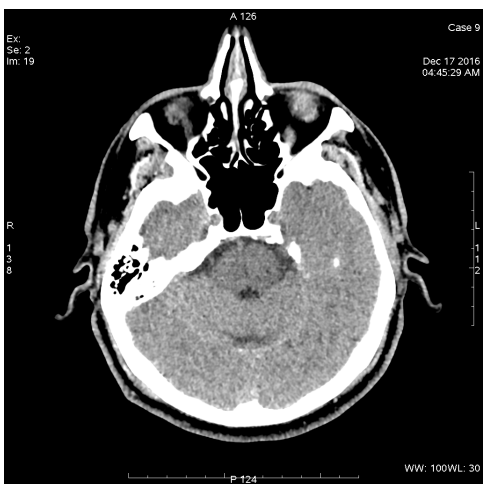
(4)



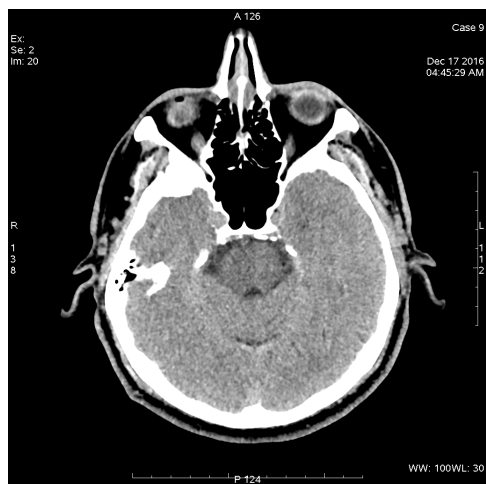
(5)



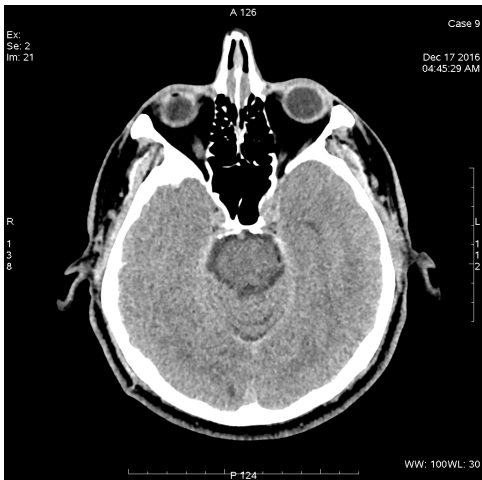
(6)



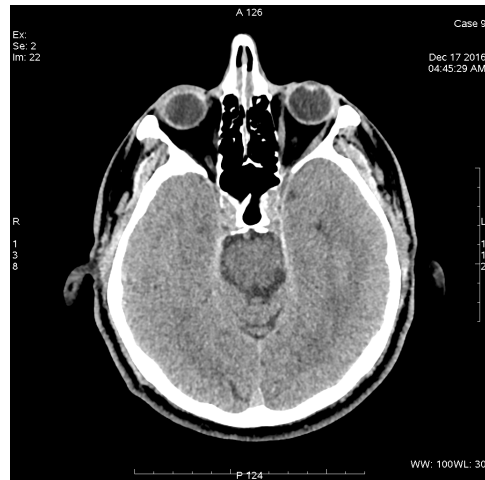
(7)



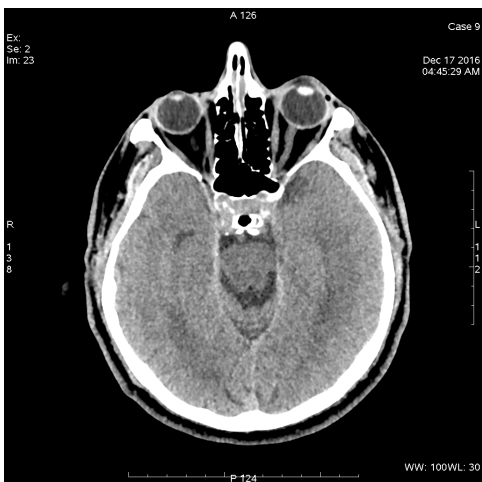
(8)



(9)



(10)



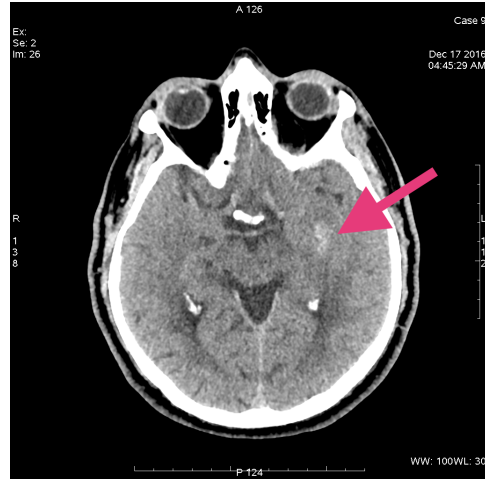
(11)



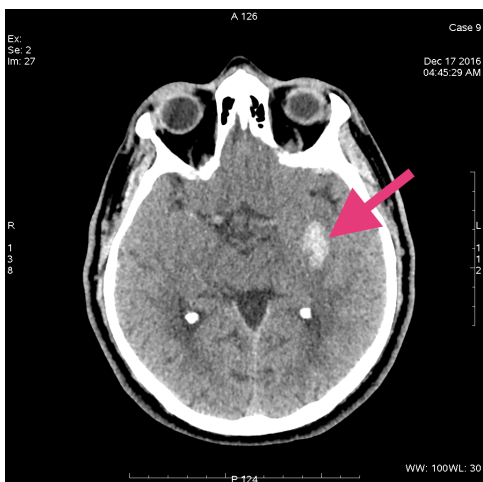
(12)



(13)



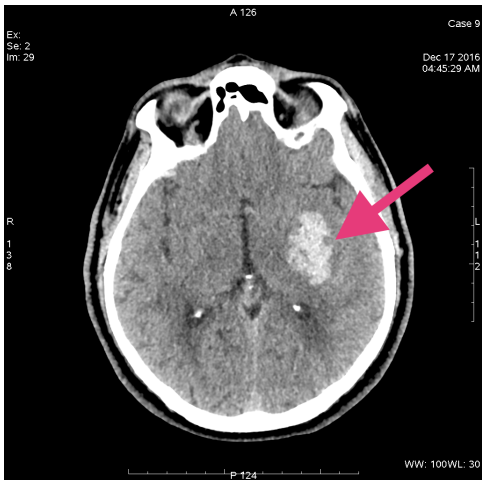
(14)



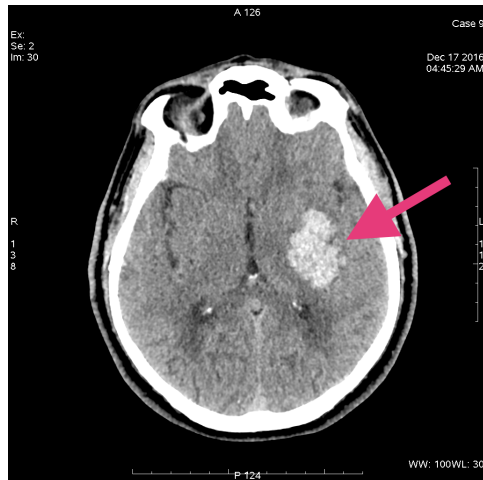
(15)



(16)



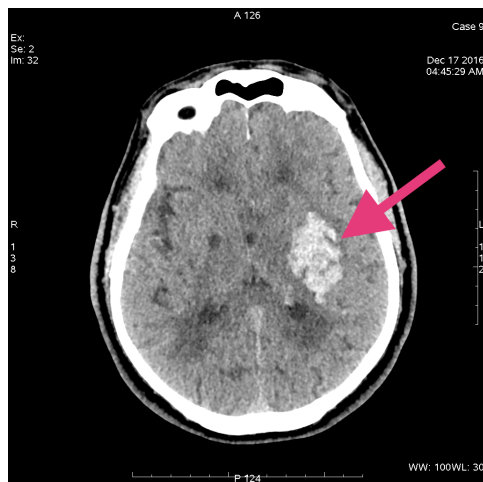
(17)



(18)



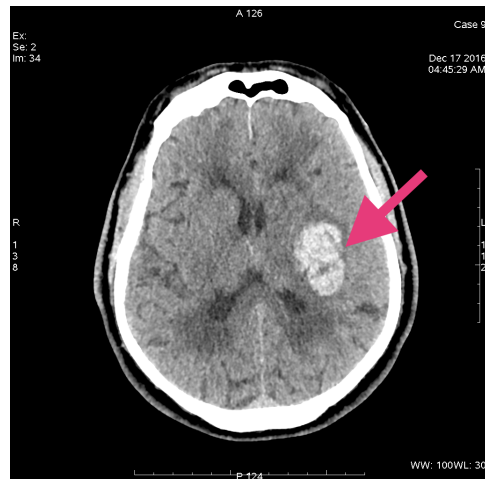
(19)



(20)



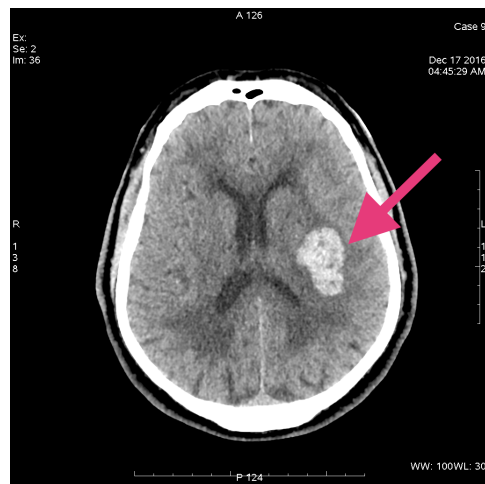
(21)



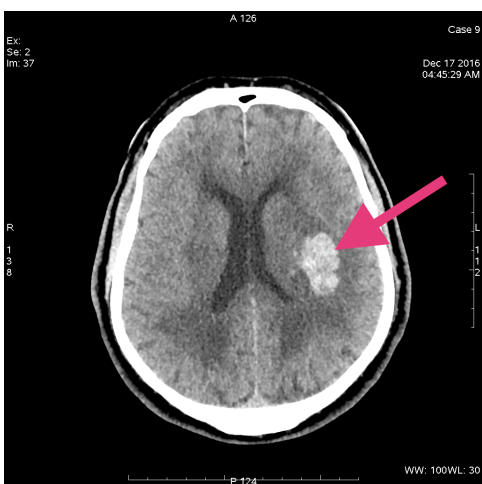
(22)



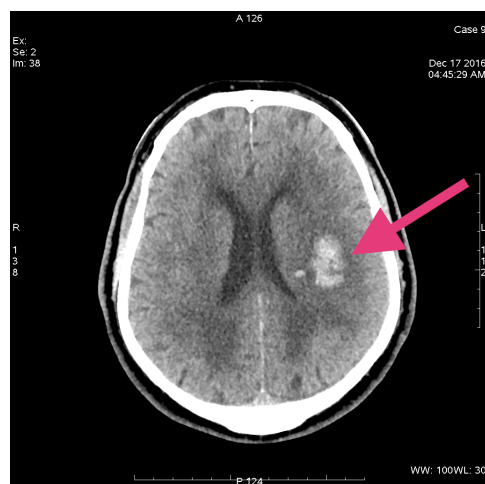
(23)



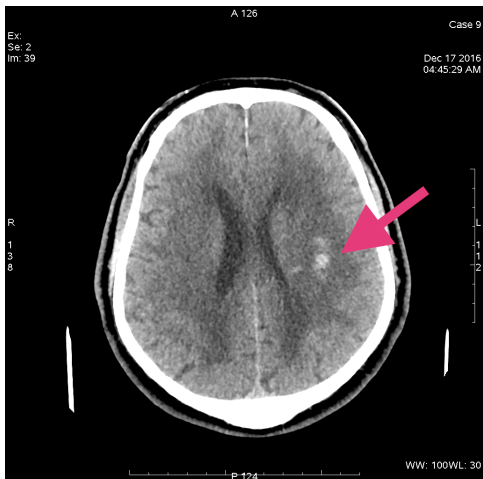
(24)



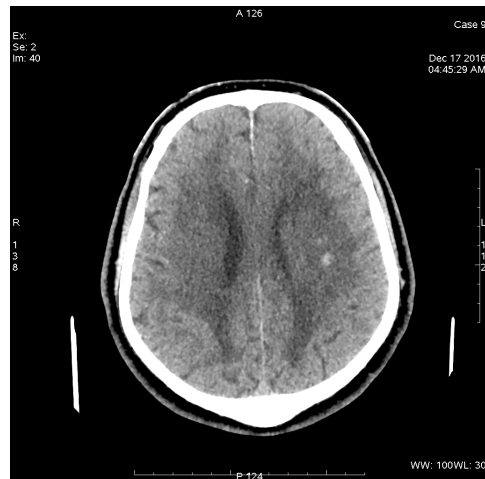
(25)



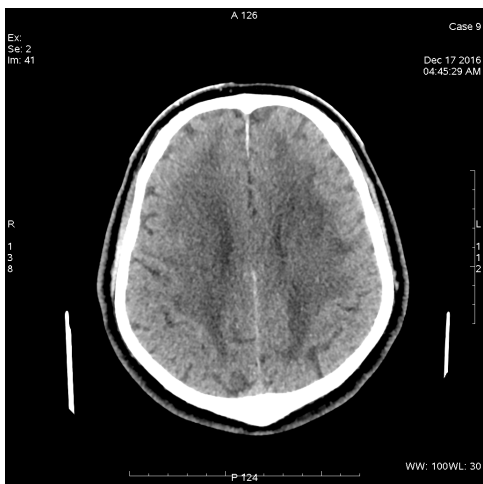
(26)



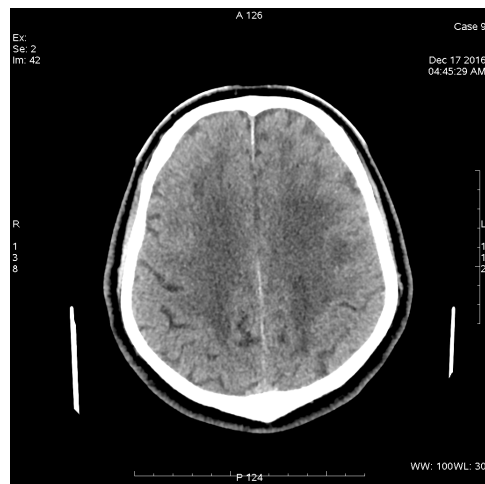
(27)



(28)



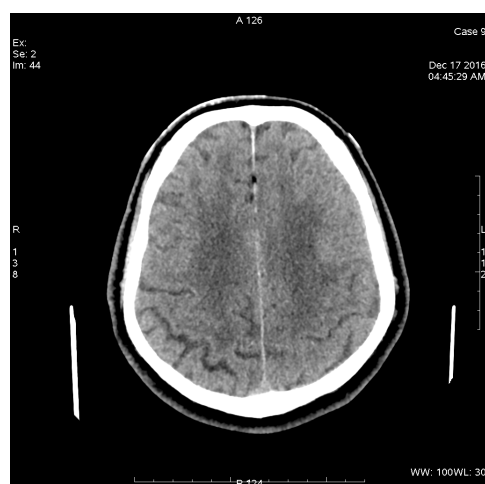
(29)



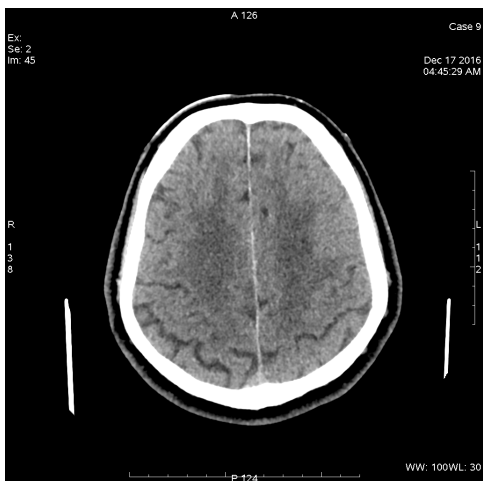
(30)



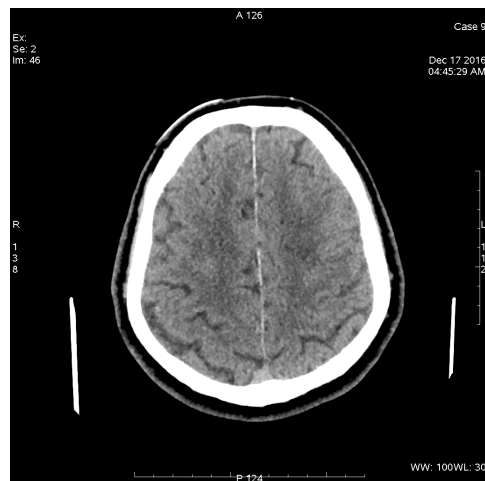
(31)



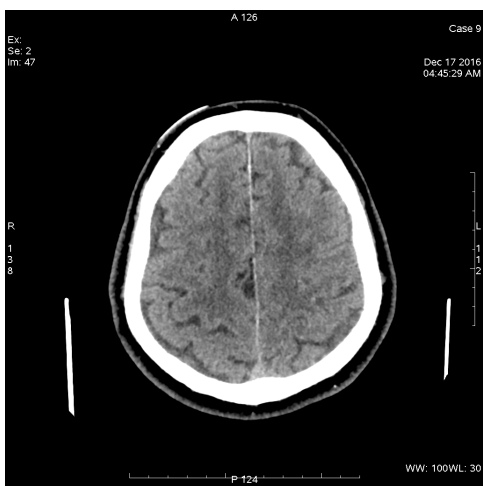
(32)



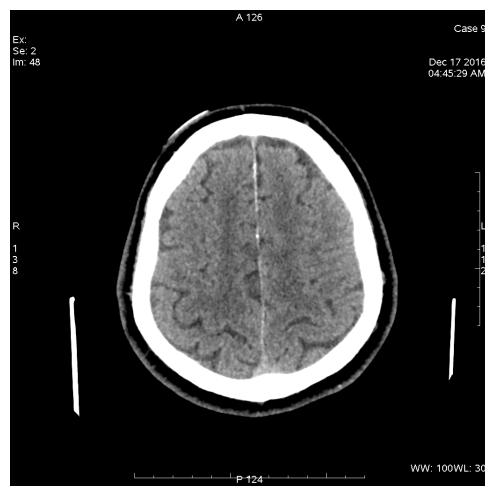
(33)



(34)



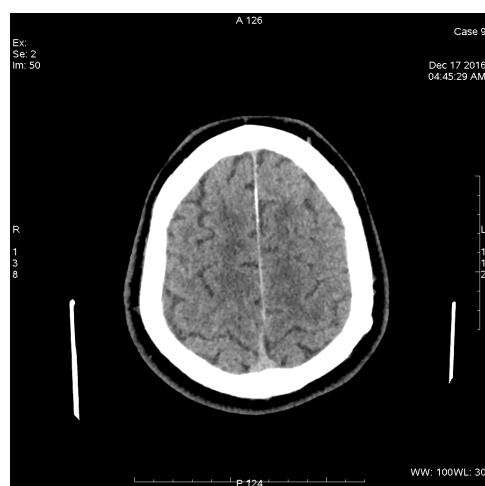
(35)



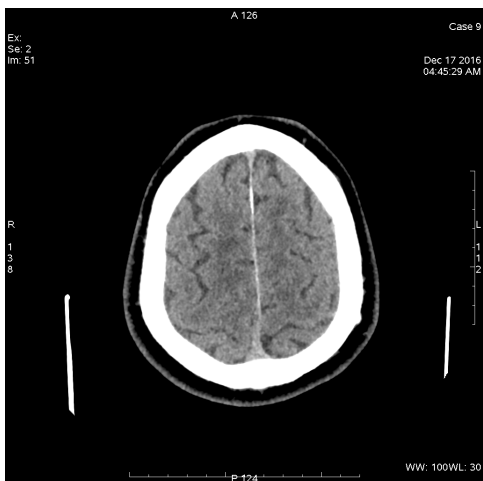
(36)



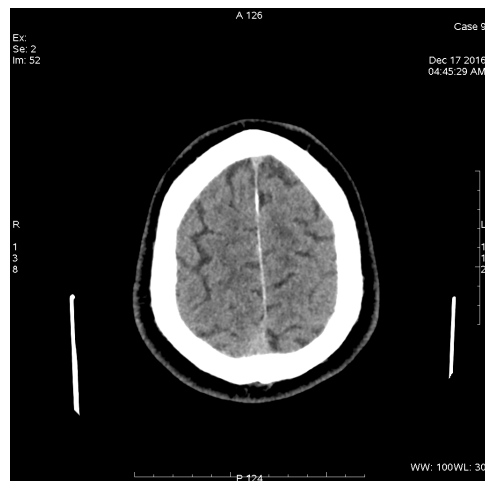
(37)



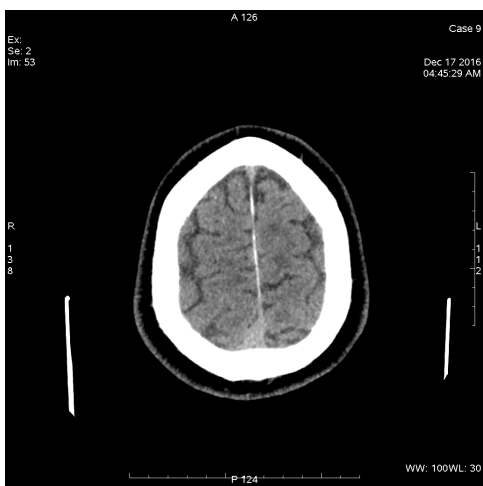
(38)



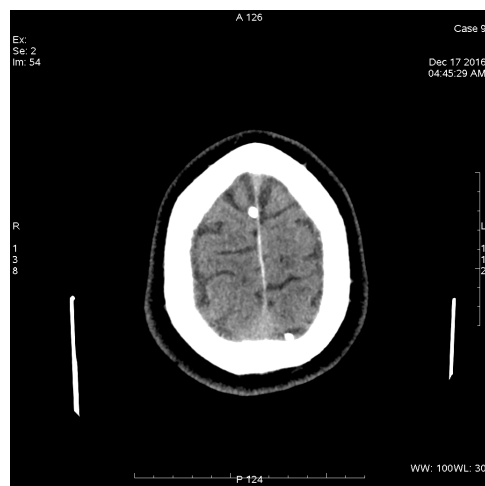
(39)



(40)



(41)



(42)



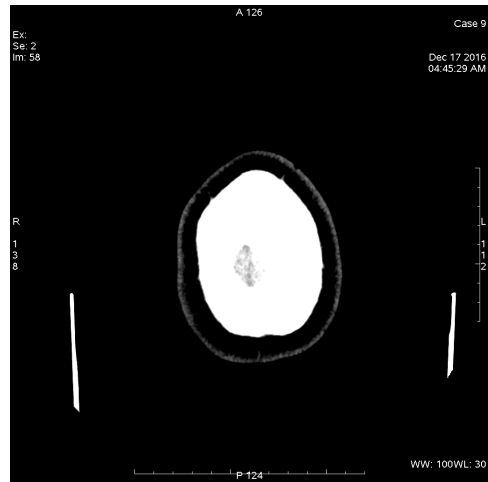
(43)



(44)



(45)



(46)

(B) Documents Pertaining to the Approval of use of CT Scans and Medical Reports from a General Hospital in Malta

Letter of Permission Sent

Undergraduate Final Year Project 2016/2017 - Permission Letter for Use of Anonymised Data

My name is John Napier and I am currently a third year University if Malta student reading a BSc ICT (Hons) in Computer Engineering. This year I will be working on my final year project which is entitled "Image Processing Techniques for Brain Haemorrhage Detection in Head CT Scans" and I will be under the supervision of Prof. Ing. Carl James Debono and co-supervised by Dr Paul Bezzina and Dr Francis Zarb. The proposal for this project is attached.

Due to the nature of the study taking place, I will be requiring anonymised CT images of the brain. Therefore I am seeking your permission and approval to obtain anonymised head CT Scan Images of patients and their corresponding anonymised examination reports. These recourses will enable me to apply image processing techniques on CT scans to detect the presence of haemorrhage in the brain, develop a curve-fitting algorithm to enclose the detected region and thanks to the examination reports evaluate the accuracy of the algorithm.

During the course of the study I will conform to the highest ethical standards as well as strict confidentiality. I also require permission from the Ethics Committee of the University of Malta in order to perform this study.

I am listing hereunder my contact details as well as those of the supervisory team should you have any queries or wish to be informed further on the nature and progress of my studies.

Prof. Ing. Carl James Debono	carl.debono@um.edu.mt	Tel No: 2340 2076
Dr Paul Bezzina	paul.bezzina@um.edu.mt	Tel No: 2340 1824
Dr Francis Zarb	francis.zarb@um.edu.mt	Tel No: 2340 1833
John Napier	john.napier.14@um.edu.mt	Tel No: 21436120 / 79436120

I thank you in advance for your kind attention.

Sincerely,

John Napier.



Permission from Hospital's Authorities

Permission from Hospital Authorities

Mr. Martoine Farrugia
Team Leader, CT Unit, Medical Imaging Department,

Mr. Joseph Castillo
Professional Lead, Medical Imaging Department,

Dr. Salvina Zrinzo
Chairperson, Medical Imaging Department

Mr. Ivan Falzon
CEO,

Ms. Sharon Young
Data Protection Officer.

DR. SALVINA ZRINZO
Consultant Radiologist
~~Chairperson~~, Medical Imaging Department
~~Mater Dei Hospital~~

INFORMATION MANAGEMENT
&
TECHNOLOGY DIRECTORATE
MATER DEI HOSPITAL
MSD 2090

Permission from Mr. Ivan Falzon (Hospital CEO)

University of Malta Mail - Hospital thesis permission

19/10/2016, 10:55



John Napier <john.napier.14@um.edu.mt>

Hospital thesis permission

Falzon Ivan at MDH-Health <ivan.falzon@gov.mt> 17 October 2016 at 20:59
To: John Napier <john.napier.14@um.edu.mt>
Cc: Zrinzo Salvina at MDH-Health <salvina.zrinzo@gov.mt>, Castillo Joseph at MDH-Health <joseph.castillo@gov.mt>, Satariano Banavage Karen at MDH-Health <karen.a.satariano-banavage@gov.mt>

Dear Mr Napier,

no objection for you to proceed in line with policies regulating such studies.

Ivan
[Quoted text hidden]

Undergraduate Final Year Project 2016/2017 - Permission Letter for Use of Anonymised Data

My name is John Napier and I am currently a third year University if Malta student reading a BSc ICT (Hons) in Computer Engineering. This year I will be working on my final year project which is entitled "Image Processing Techniques for Brain Haemorrhage Detection in Head CT Scans" and I will be under the supervision of Prof. Ing. Carl James Debono and co-supervised by Dr Paul Bezzina and Dr Francis Zarb. The proposal for this project is attached.

Due to the nature of the study taking place, I will be requiring anonymised CT images of the brain. Therefore I am seeking your permission and approval to obtain anonymised head CT Scan Images of patients and their corresponding anonymised examination reports. These recourses will enable me to apply image processing techniques on CT scans to detect the presence of haemorrhage in the brain, develop a curve-fitting algorithm to enclose the detected region and thanks to the examination reports evaluate the accuracy of the algorithm.

During the course of the study I will conform to the highest ethical standards as well as strict confidentiality. I also require permission from the Ethics Committee of the University of Malta in order to perform this study.

I am listing hereunder my contact details as well as those of the supervisory team should you have any queries or wish to be informed further on the nature and progress of my studies.

Prof. Ing. Carl James Debono	carl.debono@um.edu.mt	Tel No: 2340 2076
Dr Paul Bezzina	paul.bezzina@um.edu.mt	Tel No: 2340 1824
Dr Francis Zarb	francis.zarb@um.edu.mt	Tel No: 2340 1833
John Napier	john.napier.14@um.edu.mt	Tel No: 21436120 / 79436120

I thank you in advance for your kind attention.

Sincerely,

John Napier.

Permission from Ms. Sharon Young (Data Protection Officer)

University of Malta Mail - Thesis Hospital Permission

16/10/2016, 14:14



John Napier <john.napier.14@um.edu.mt>

Thesis Hospital Permission

Data Protection at MDH <datapro.mdh@gov.mt> 16 October 2016 at 13:38
To: John Napier <john.napier.14@um.edu.mt>
Cc: Aquilina Graziella at MDH-Health <graziella.aquilina@gov.mt>, Buhagiar Nadine at MDH-Health <nadine.buhagiar@gov.mt>

Dear Mr Napier

On the basis of the documentation you submitted, from the MDH data protection point of view you have been cleared to proceed with your study provided that you obtain approval from MDH CEO and the University Ethics Committee.

Please contact Ms. Nadine Buhagiar on 2545 5334 or Ms. Graziella Aquilina on 2545 5346 to present a copy of your approvals and fill in the appropriate Data Protection Form.

Remember that in no way should you retain any personal details you obtain from your research and this should be destroyed at the end of your study.

All medical records are to be viewed at the Medical Records Department MDH.

You are requested to submit a copy of your findings to this office at the end of your study.

Regards

Sharon Young

Data Protection Officer



T +356 +356 25455340

E simon.caruana@gov.mt

Mater Dei Hospital, Triq tal-Qroqq, Msida, Malta MSD 2090 | Tel +356 2545 0000 | www.mdh.gov.mt

Data Protection Declaration



Human Resources & Administration Directorate
Administration Block, Room A210092
Mater Dei Hospital
Msida MSD 2090
Telephone: 2545 4137

DECLARATION BY VISITING STUDENTS

I hereby declare that I will respect the confidentiality and privacy of any personal data or information that I might come across during my attachment at Mater Dei Hospital and will in no circumstance disclose any such information. I also confirm that I am aware of the provisions of the Data Protection Act and that I will abide by all Government and hospital regulations related to data.

I am also aware that I will be assigned a mentor for the duration of my attachment and will abide by the directions given by the same mentor.

Details of student

Signature: John Napier
Full name: John Napier
ID number: 970964
Educational Institution: University of Malta
Date: 17/10/16

Endorsement by Parent/Guardian (where applicable)

Signature: _____
Full name: _____
ID number: _____
Date: _____

Disclaimer: Mater Dei Hospital will not be, under any circumstance, liable for consequential or incidental damages that might arise out of or related to the behaviour of the said student vis-à-vis the above instructions.

Data Protection Statement: The personal data supplied on this form will be processed in accordance with the Data Protection Act, XXXVI of 2001.

HRA/1043/01.0

INFORMATION MANAGEMENT
&
TECHNOLOGY DIRECTORATE
MATER DEI HOSPITAL
MSD 2090

[Signature]
17.10.16

Permission by the University of Malta's Research Ethics Committee

University of Malta Mail - ICT010/2016 - UREC Response

16/11/2016, 23:34



UNIVERSITY OF MALTA
L-Università ta' Malta

John Napier <john.napier.14@um.edu.mt>

ICT010/2016 - UREC Response

Helen Grech <helen.grech@um.edu.mt>

12 November 2016 at 16:55

To: Vanessa Marie Sammut Borg <vanessa.m.borg@um.edu.mt>

Cc: Michelle Caruana Montebello <michelle.montebello@um.edu.mt>, John Napier <john.napier.14@um.edu.mt>, Carl James Debono <carl.debono@um.edu.mt>, Conrad Attard <conrad.attard@um.edu.mt>

Dear Mr Napier,

Your proposed study is approved.

Good luck with the study.

Sincerely

Helen Grech

*Professor Helen Grech
Chairperson, University Research Ethics Committee
Head, Department of Communication Therapy
Deputy Dean, Faculty of Health Sciences
University of Malta, MSD 2090
Tel: +356 2340 1858*